Supporting information for the manuscript:

Exploring the reductive CO_2 fixation with amines and hydrosilanes using readily available Cu(II) NHC–phenolate catalyst precursors

Giammarco Meloni, [a,b] Luca Morgan, [a] David Cappelletti, [a] Matteo Bevilacqua, [a] Claudia Graiff, [c] Piermaria Pinter, [d] Andrea Biffis, [a,b] Cristina Tubaro, *[a,b] and Marco Baron *[a,b]

a. Dipartimento di Scienze Chimiche, Università degli Studi di Padova, via Marzolo 1, 35131 Padova, Italy.

b. Consorzio Interuniversitario per la Reattività Chimica e la Catalisi, Unità di Ricerca di Padova, via Marzolo 1, 35131 Padova, Italy.

c. Dipartimento di Scienze Chimiche, della Vita e della Sostenibilità Ambientale, Università degli Studi di Parma, Parco Area delle Scienze 17/A, 43124 Parma, Italy.

d. Novaled GmbH, Elisabeth-Boer-Straße 9, 01099 Dresden, Germany.

* marco.baron@unipd.it

C O N T E N T S

1. ^{1}H NMR spectra

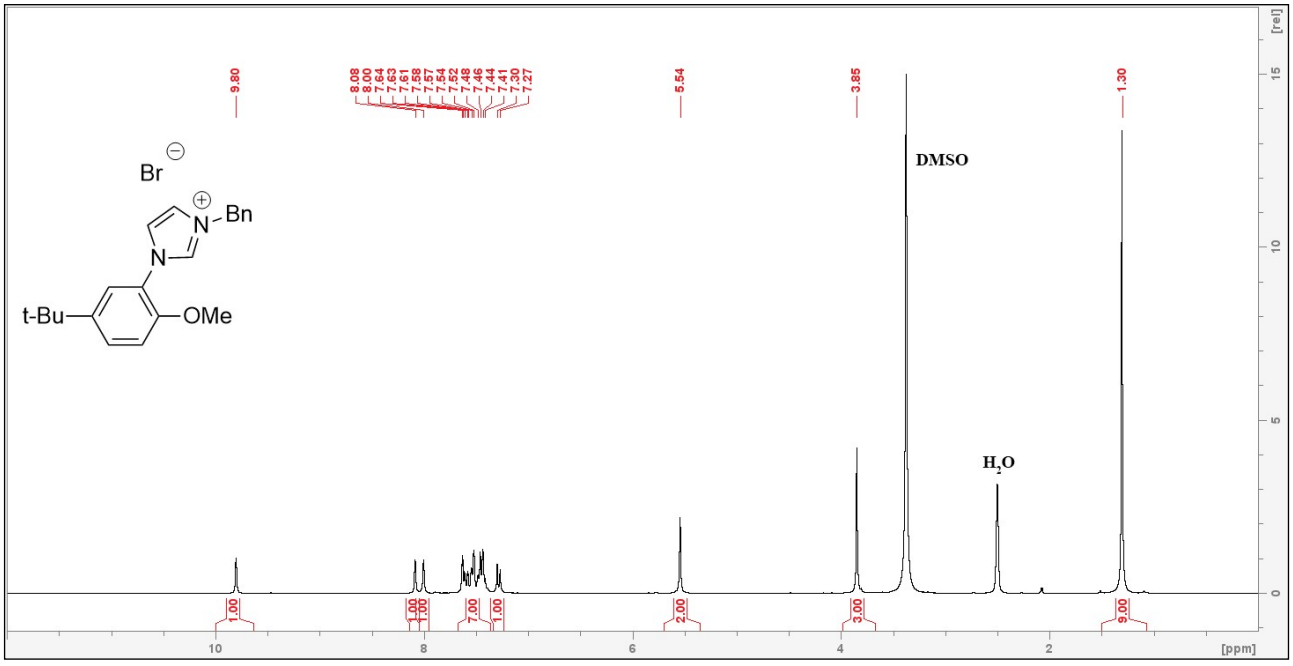

Figure S1. ^{1}H NMR spectra of **Ha^{1}Br** in DMSO–d_6.

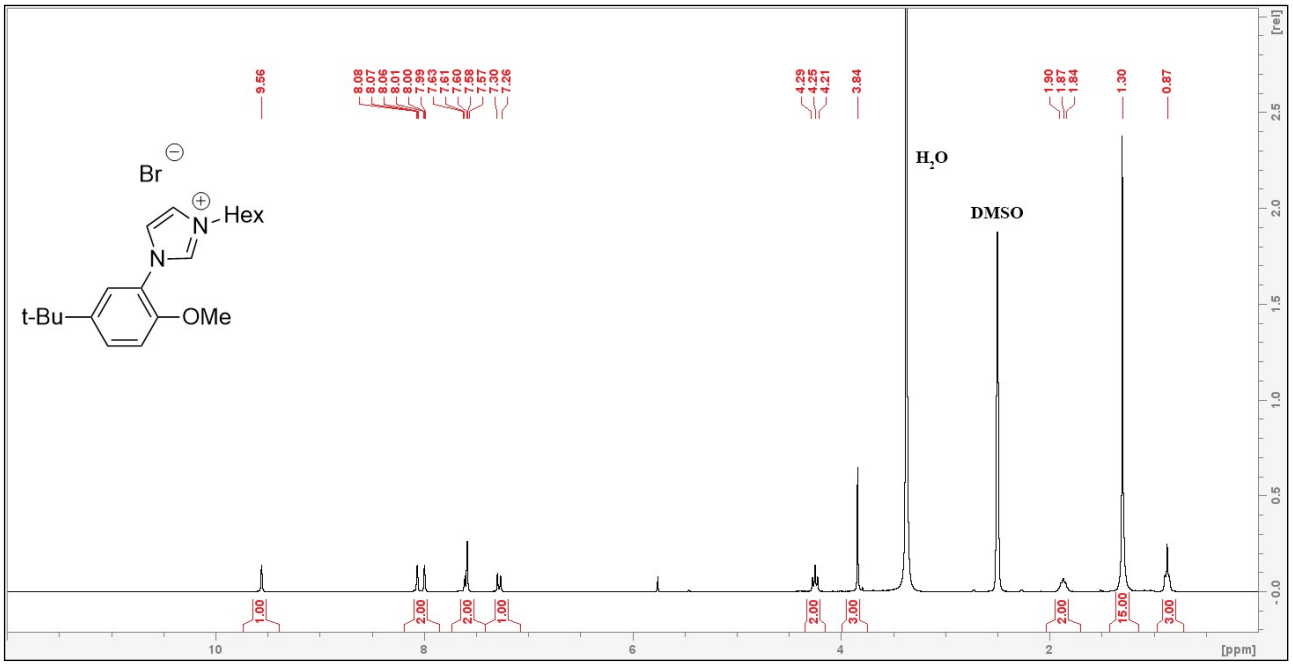

Figure S2. ^{1}H NMR spectra of **Ha^{2}Br** in DMSO–d_6.

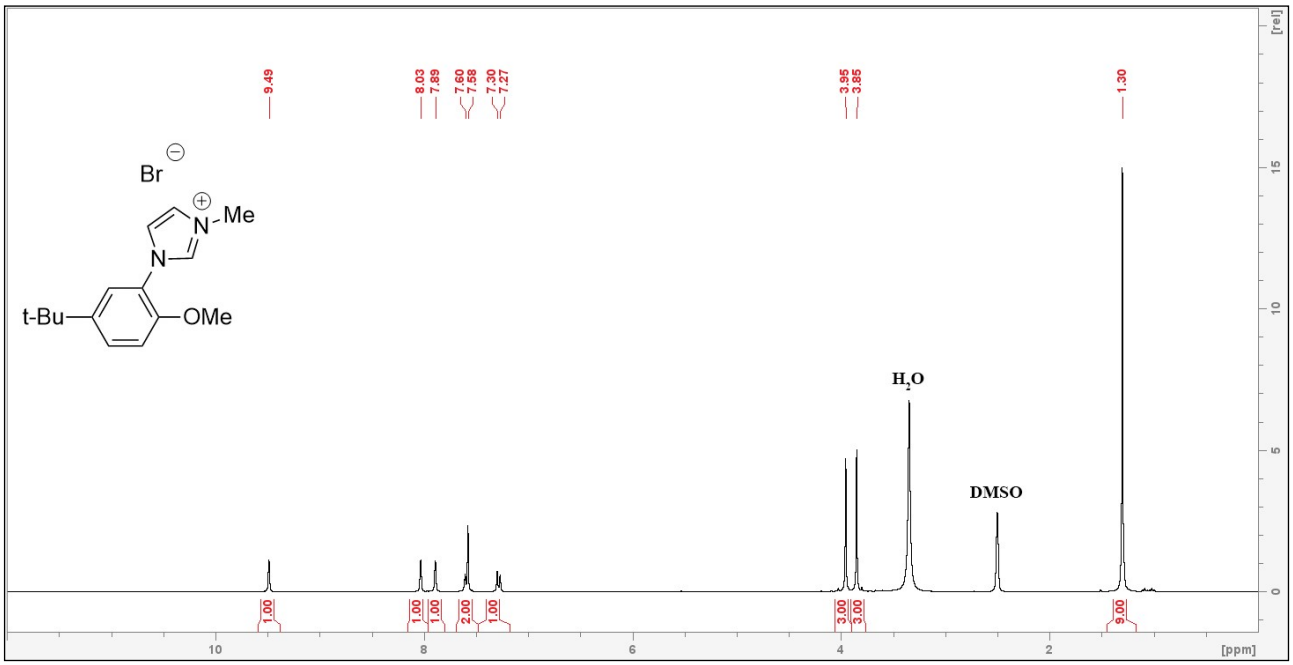

Figure S3. ^{1}H NMR spectra of **Ha^{3}Br** in DMSO–d_6.

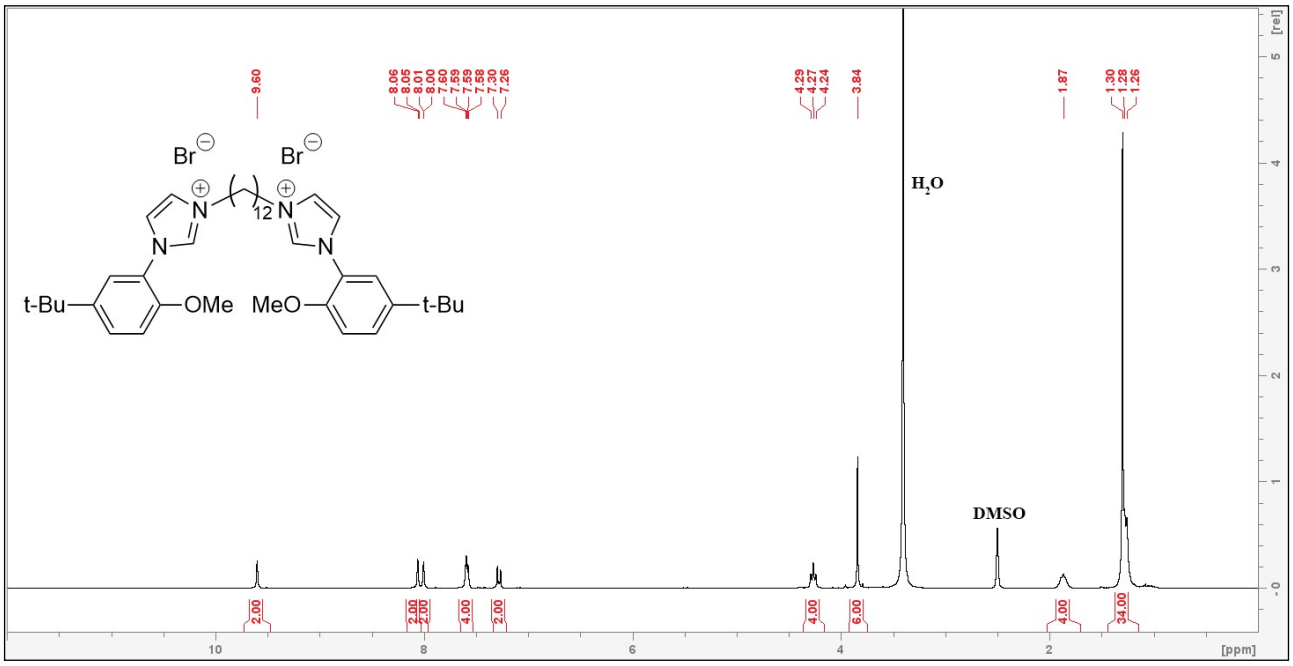

Figure S4. ^{1}H NMR spectra of **H_2a^{4}Br$_2$** in DMSO–d_6.

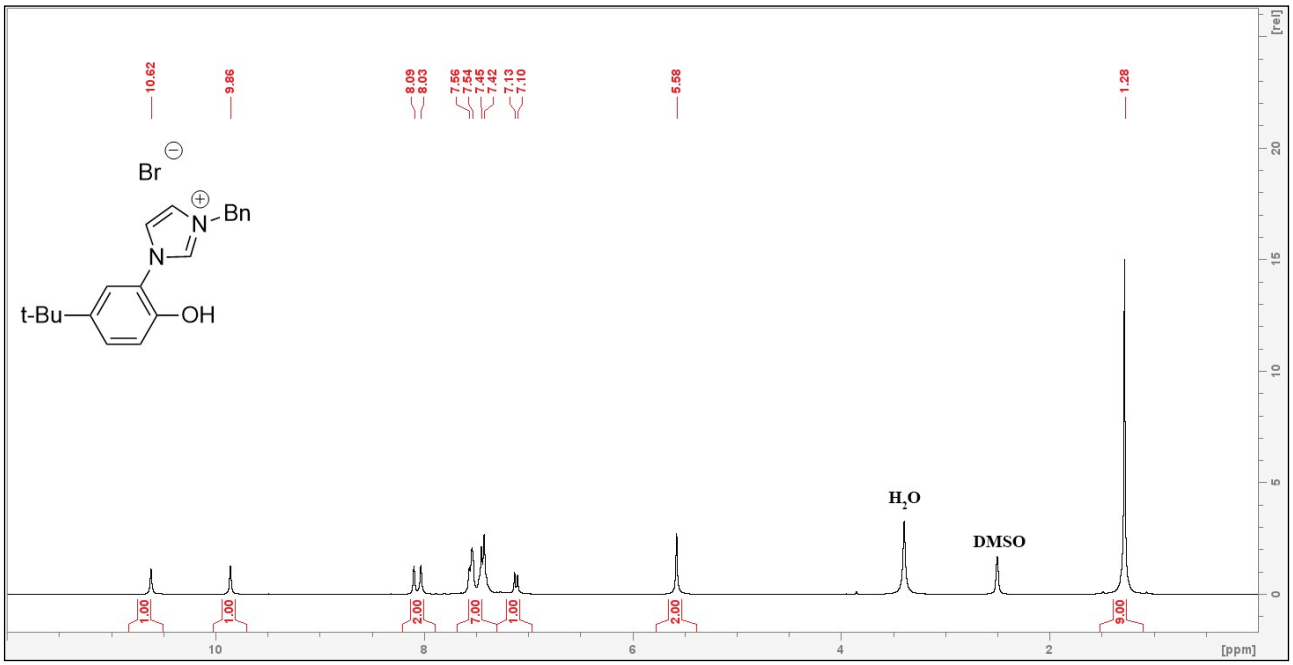

Figure S5. ^{1}H NMR spectra of **H_2L^1Br** in DMSO–d_6.

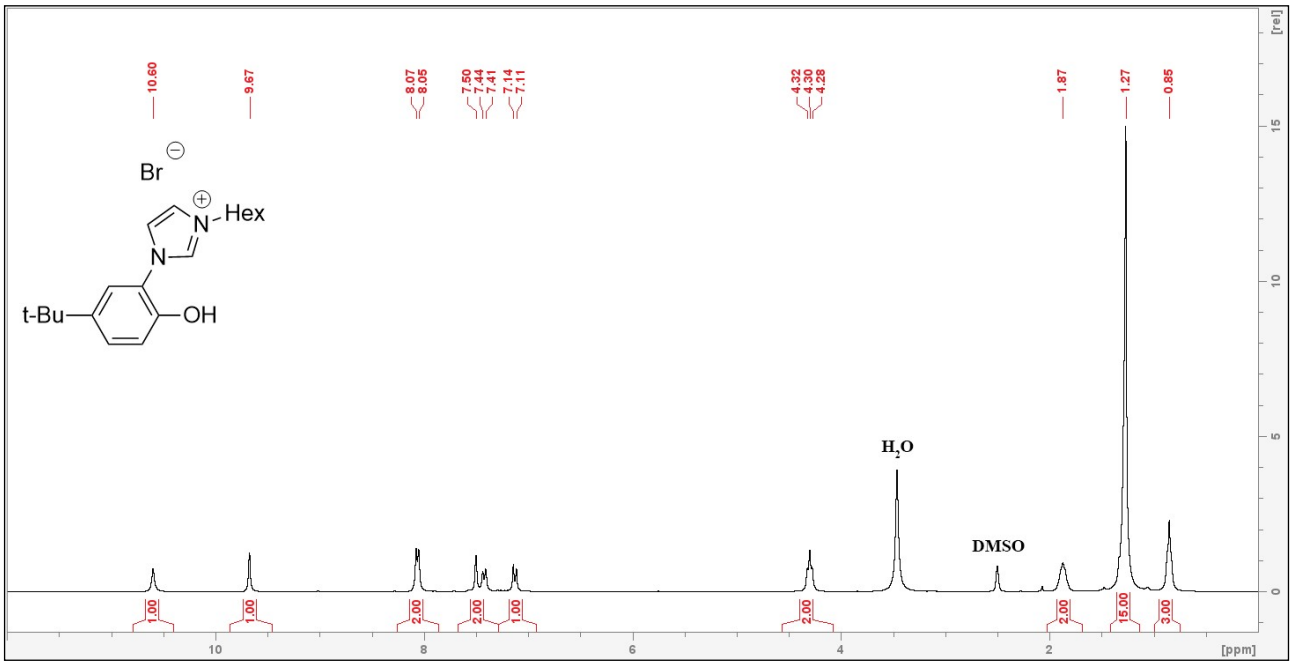

Figure S6. ^{1}H NMR spectra of **H_2L^2Br** in DMSO–d_6.

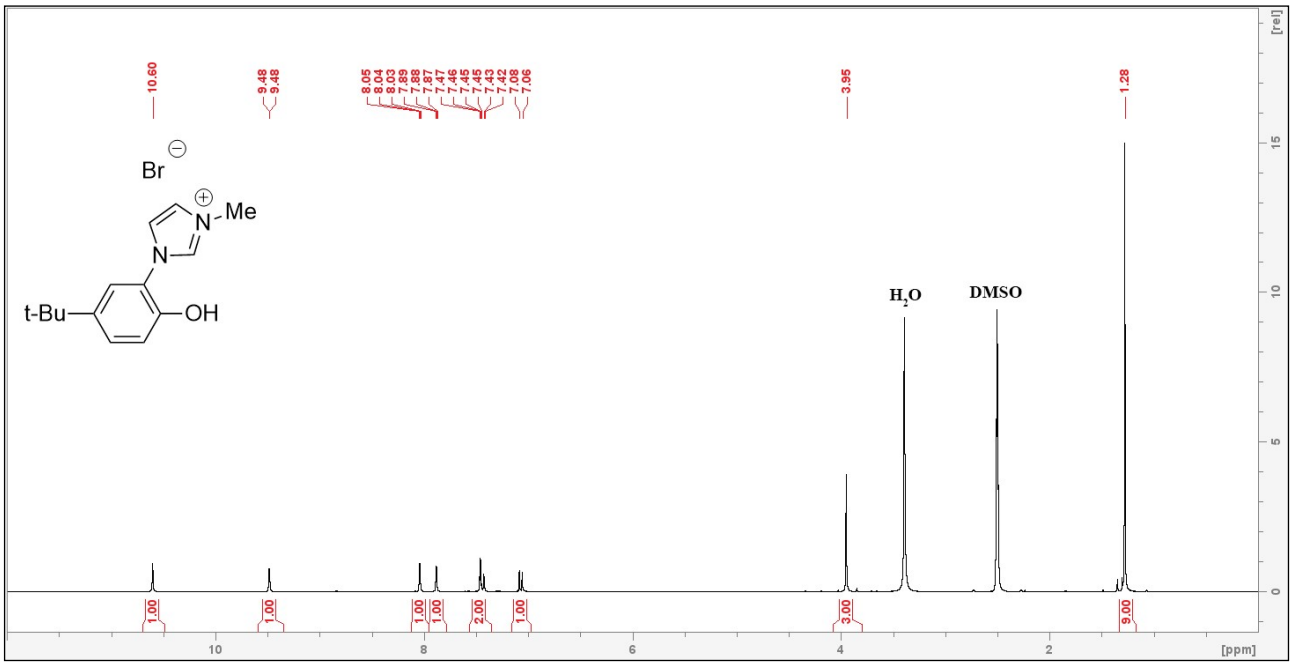

Figure S7. ^{1}H NMR spectra of **H_2L^3Br** in DMSO–d_6.

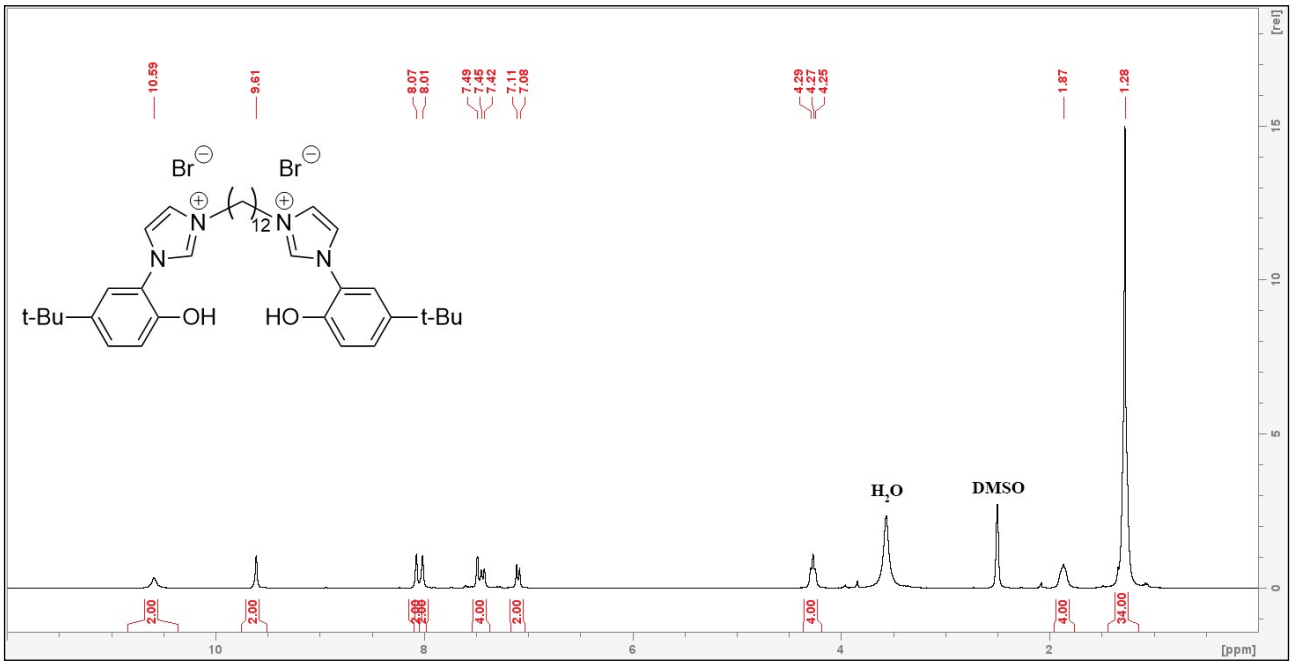

Figure S8. ^{1}H NMR spectra of **$H_4L^4Br_2$** in DMSO–d_6.

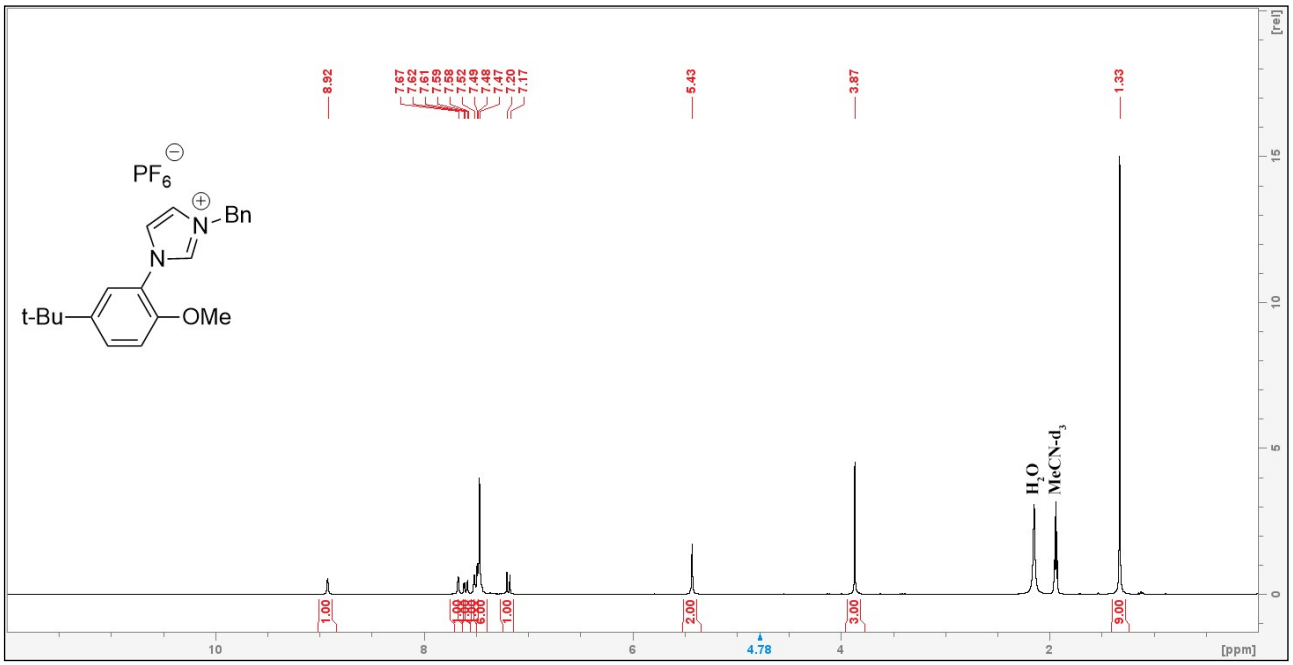

Figure S9. ^{1}H NMR spectra of **Ha^{1}PF$_6$** in CD_3CN.

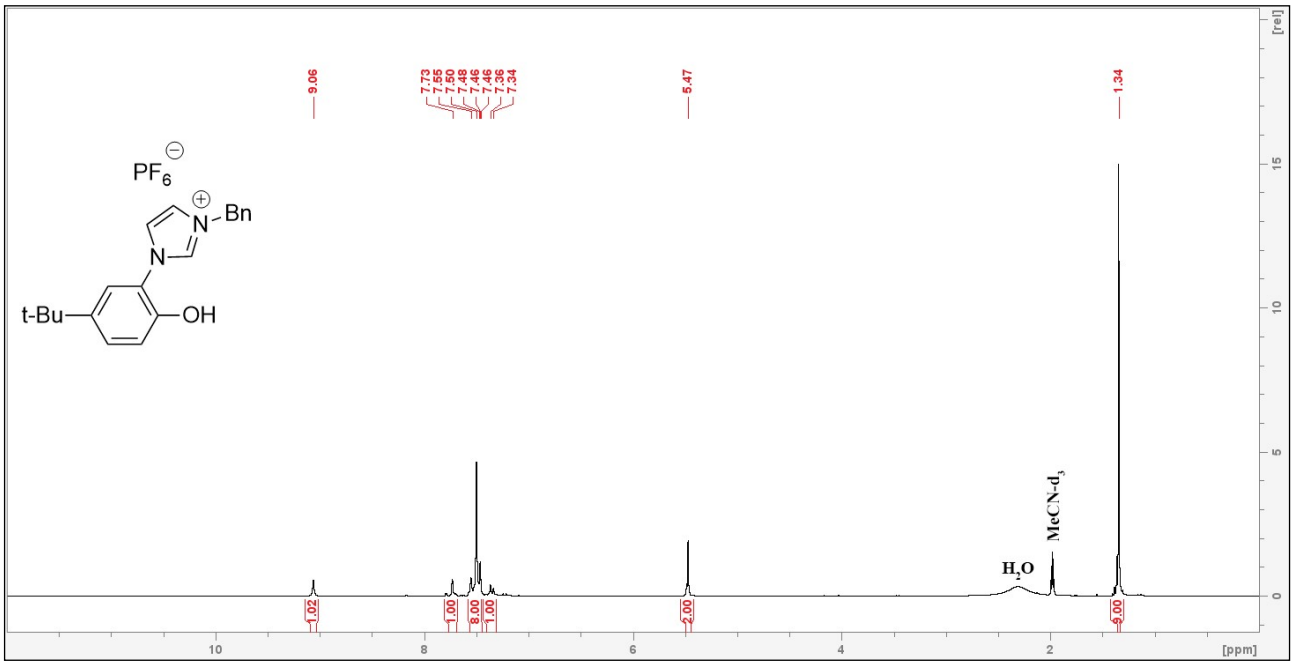

Figure S10. ^{1}H NMR spectra of **H$_2$L^{1}PF$_6$** in CD_3CN.

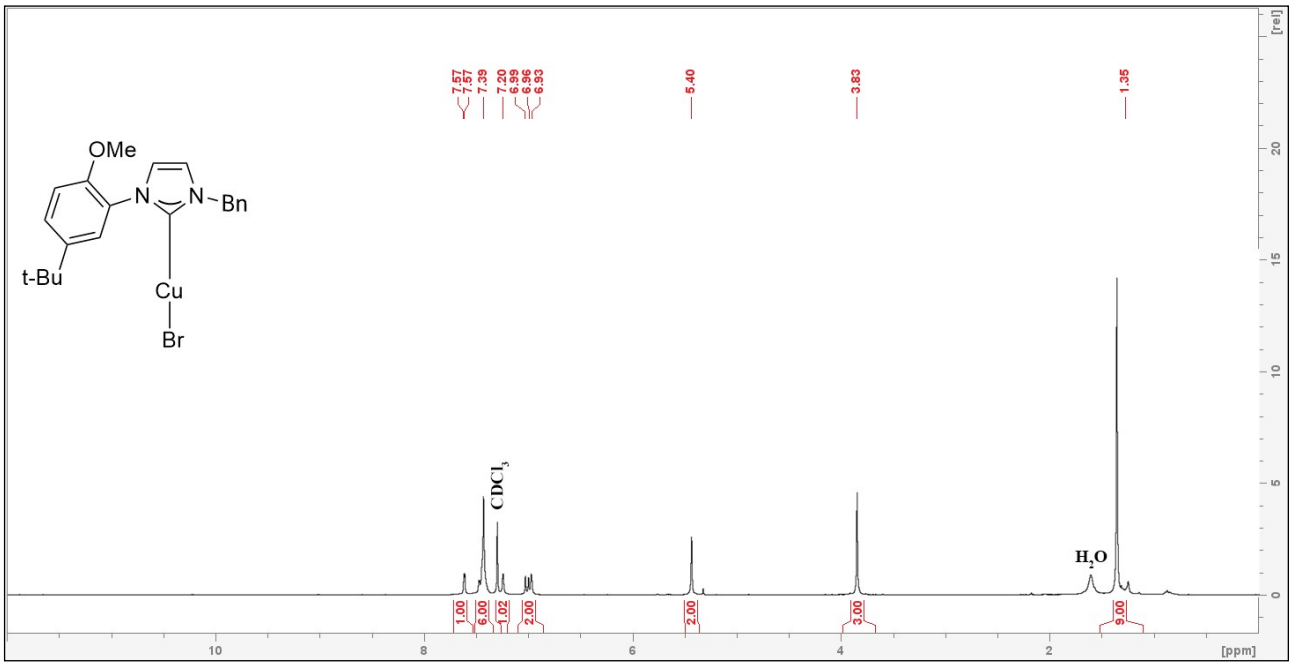

Figure S11. ^{1}H NMR spectra of **[CuBr(a^{1})]** in $CDCl_3$.

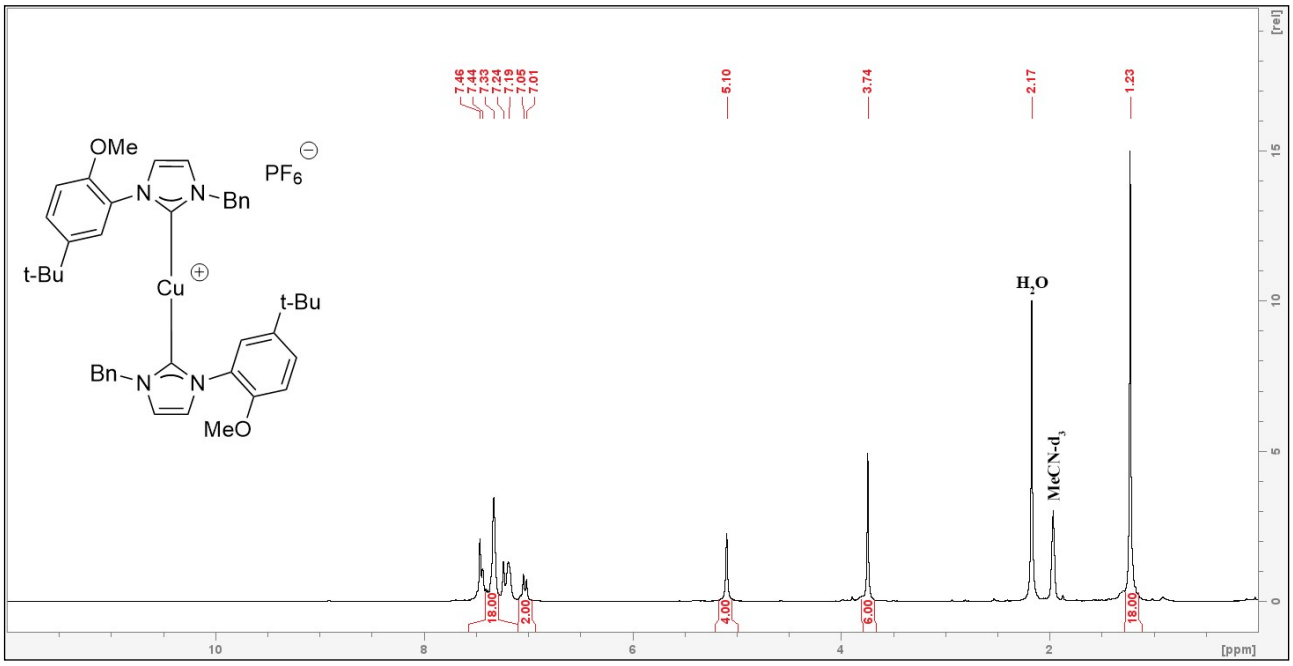

Figure S12. ^{1}H NMR spectra of **[Cu(a^{1})$_2$]PF$_6$** in CD_3CN.

2. ^{13}C NMR spectra

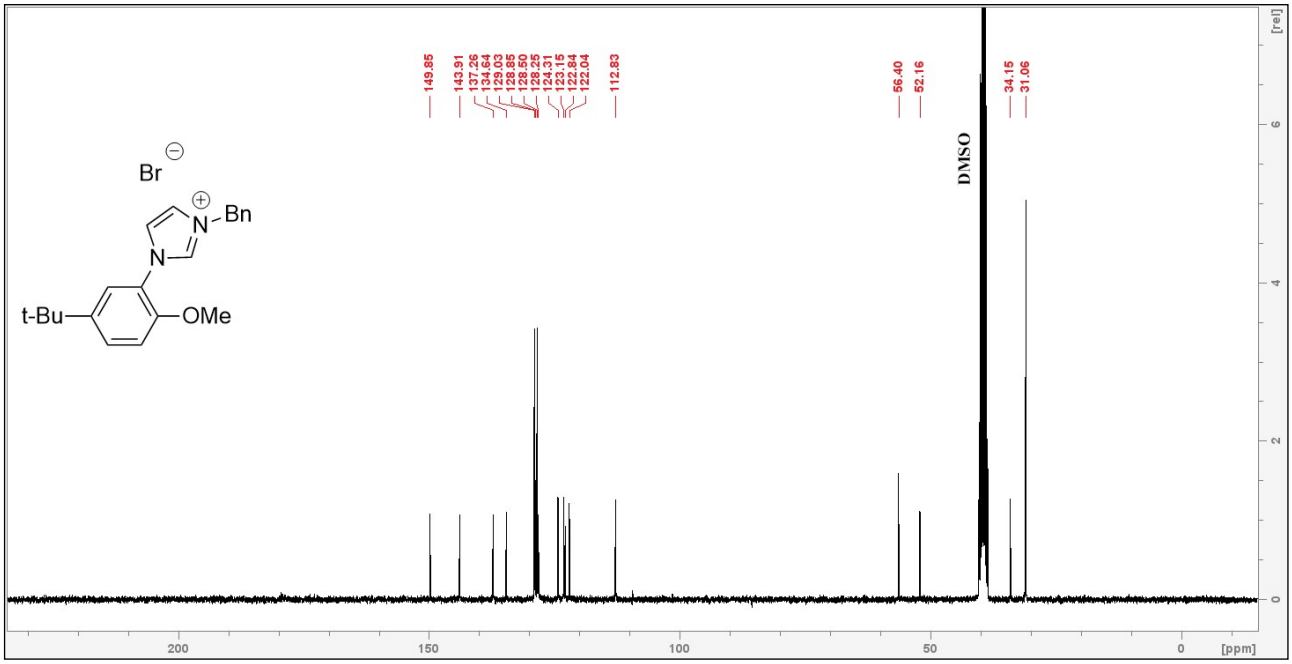

Figure S13. ^{13}C NMR spectra of **Ha^{1}Br** in DMSO–d_6.

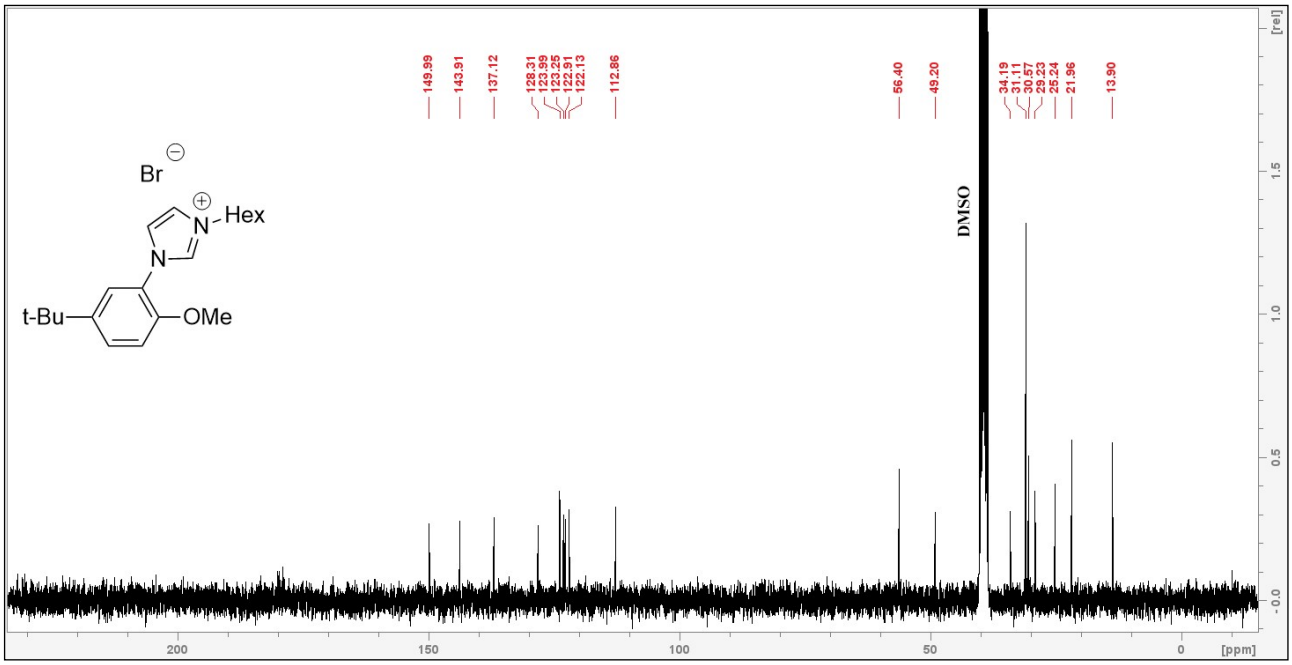

Figure S14. ^{13}C NMR spectra of **Ha^{2}Br** in DMSO–d_6.

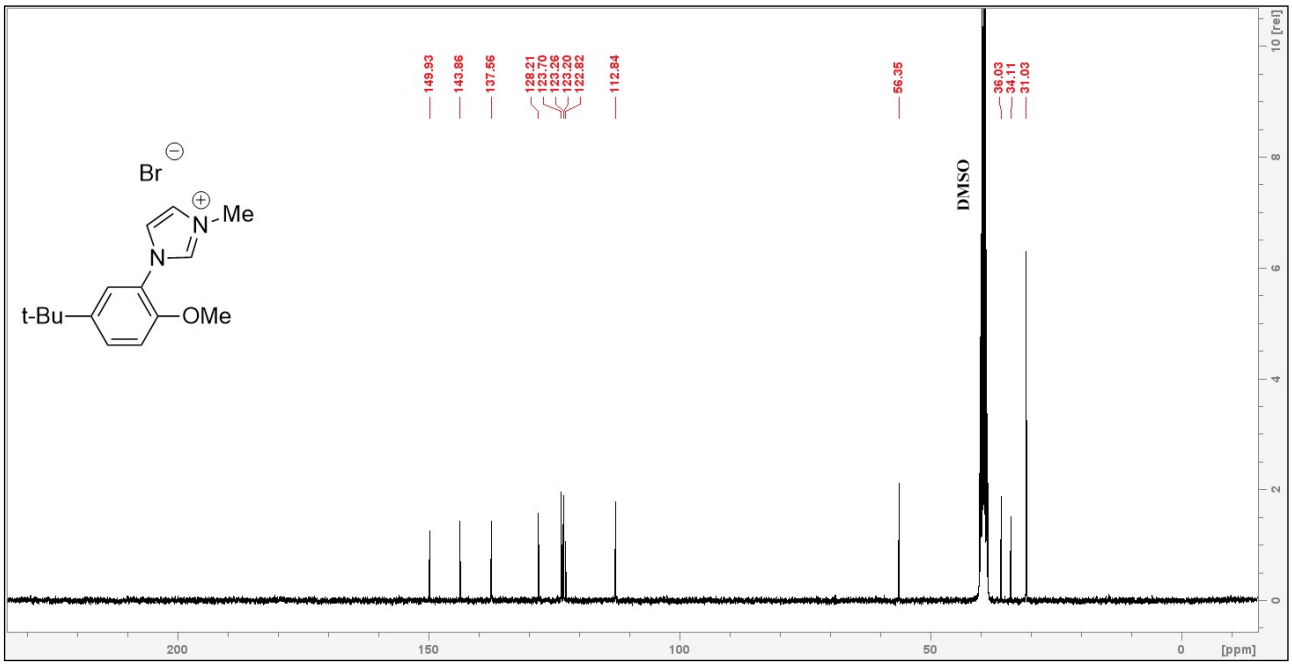

Figure S15. ^{13}C NMR spectra of **Ha^{3}Br** in DMSO–d_6.

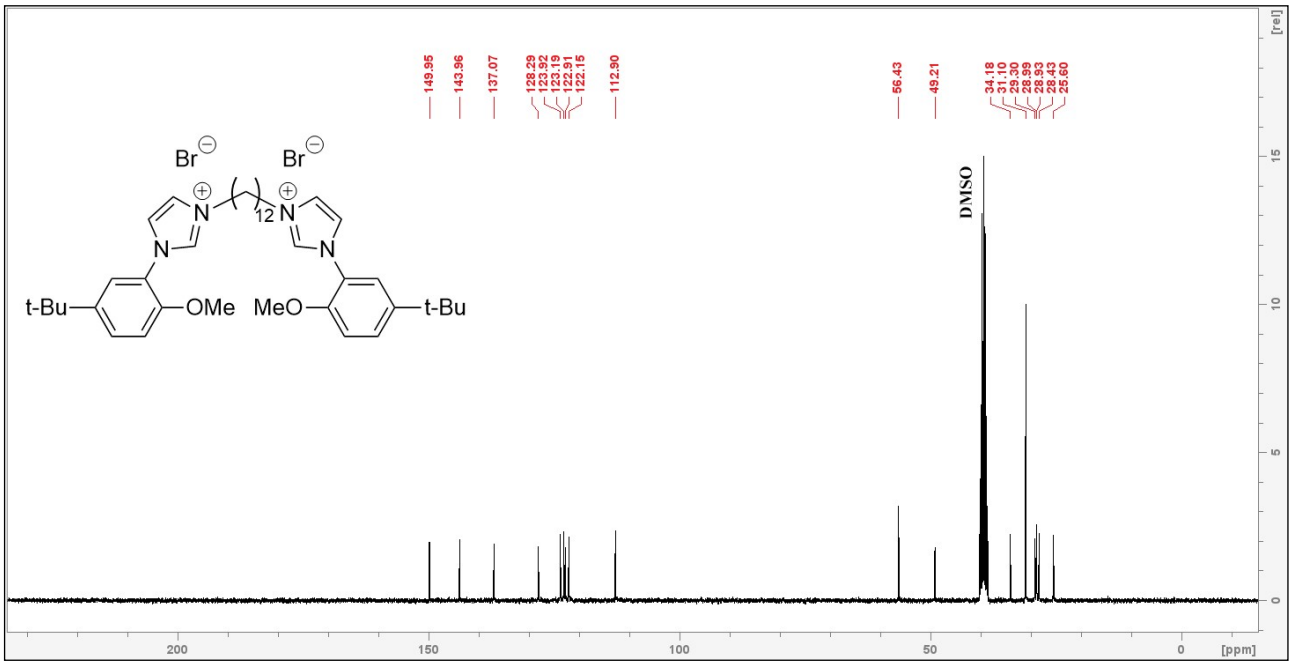

Figure S16. ^{13}C NMR spectra of **H_2a^{4}Br$_2$** in DMSO–d_6.

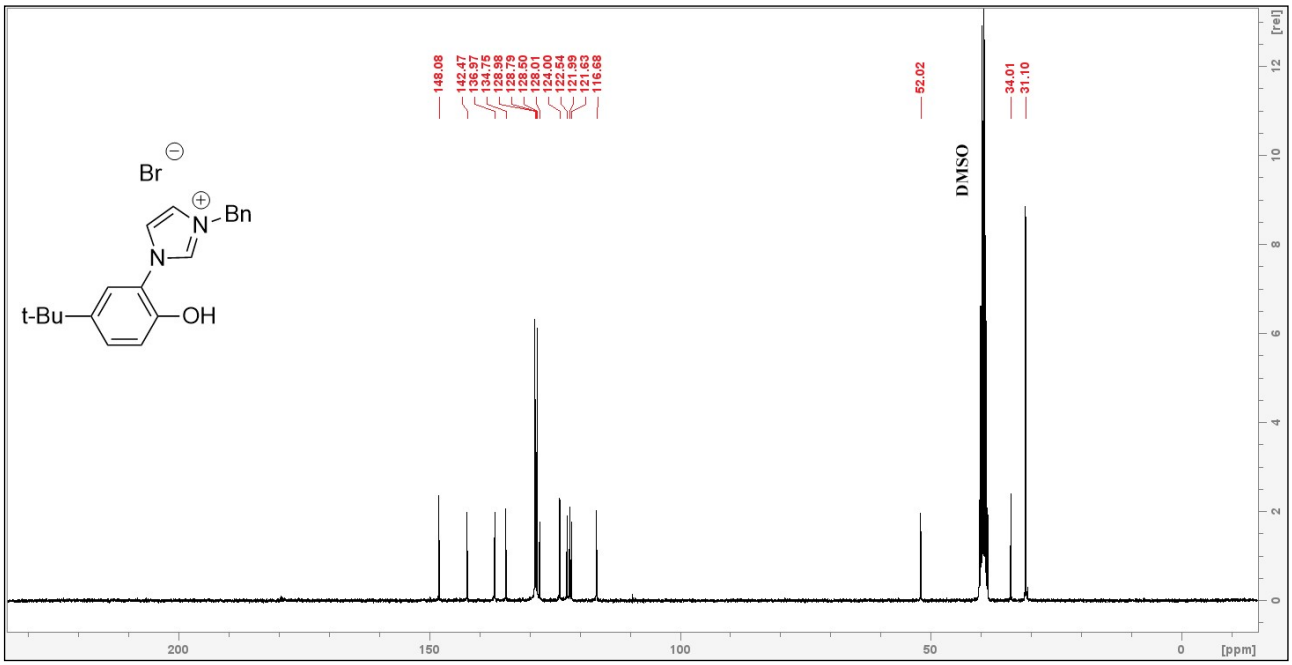

Figure S17. ^{13}C NMR spectra of **H_2L^1Br** in DMSO–d_6.

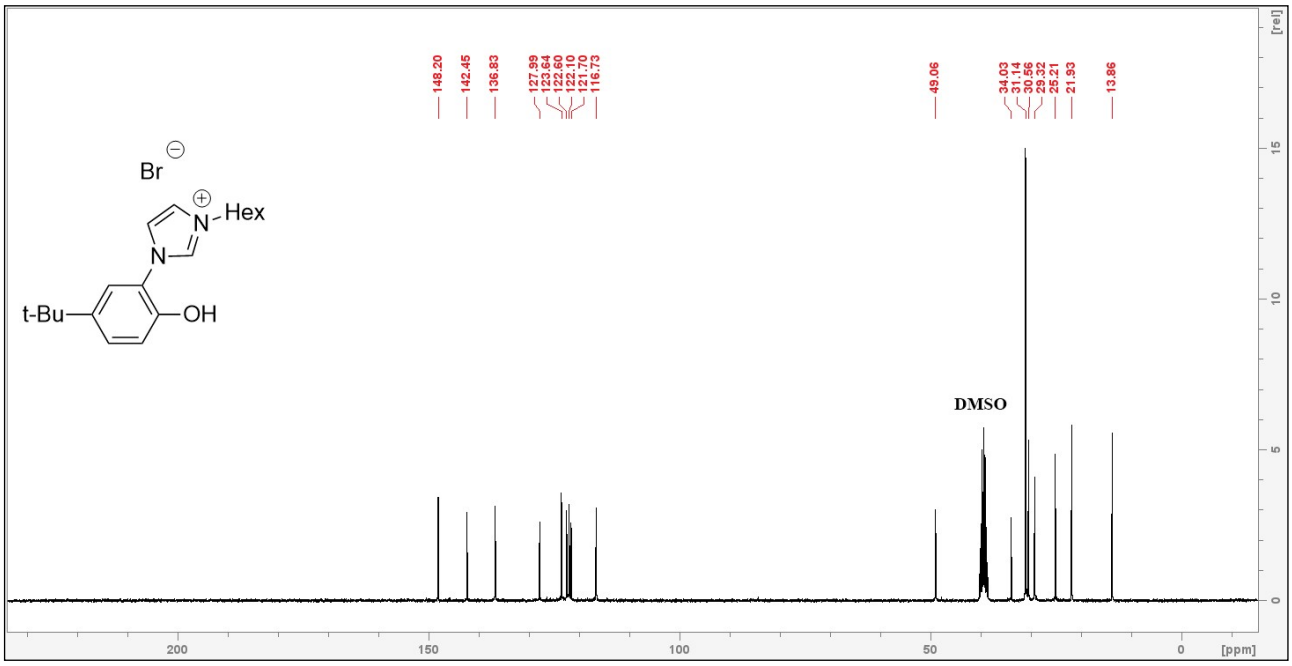

Figure S18. ^{13}C NMR spectra of **H_2L^2Br** in DMSO–d_6.

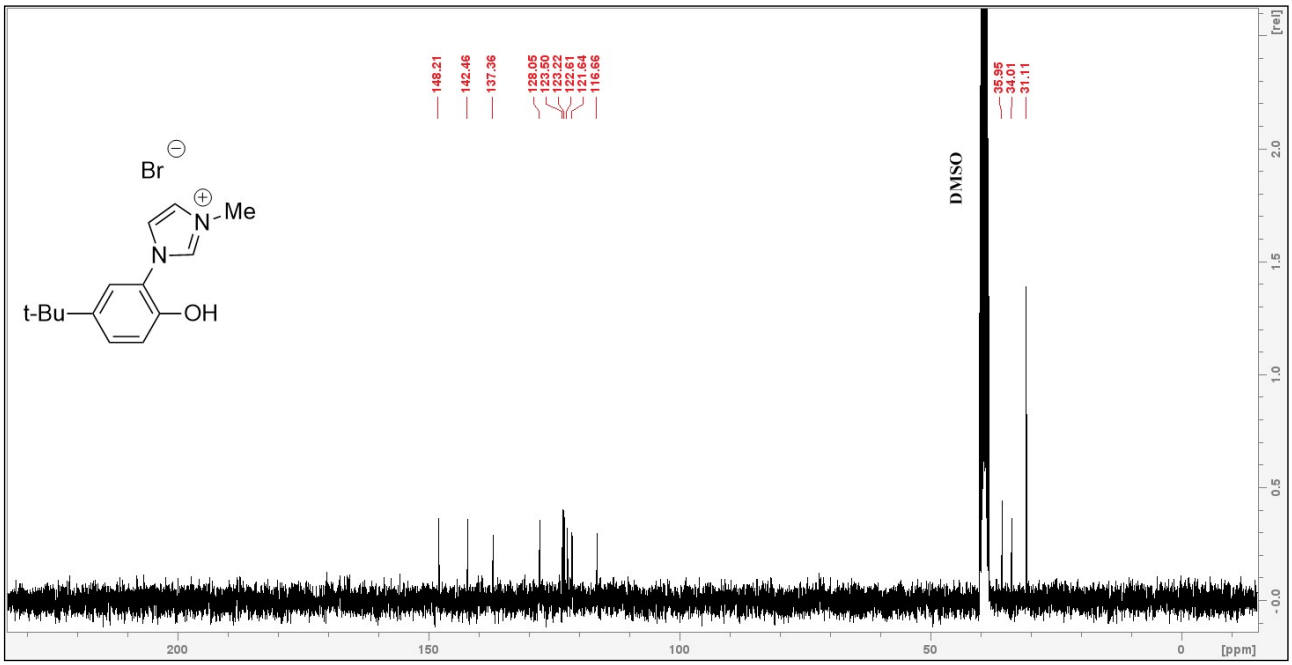

Figure S19. ^{13}C NMR spectra of **H_2L^3Br** in DMSO–d_6.

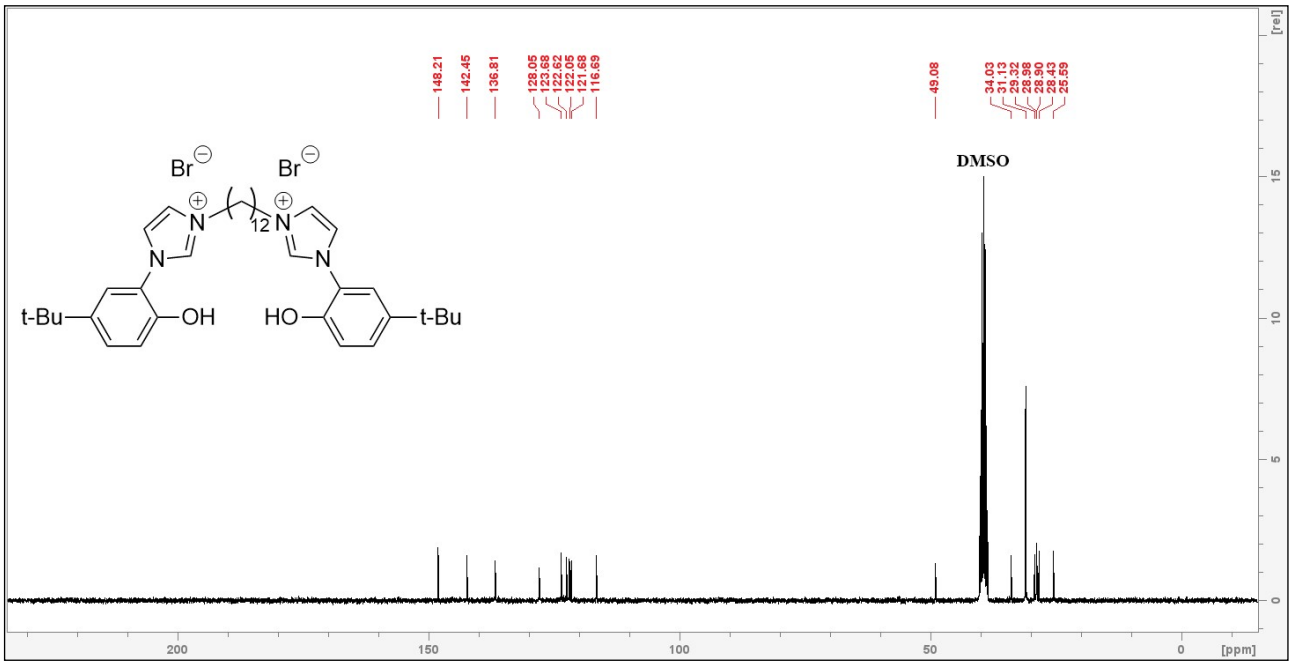

Figure S20. ^{13}C NMR spectra of **$H_4L^4Br_2$** in DMSO–d_6.

3. ^{31}P NMR spectra

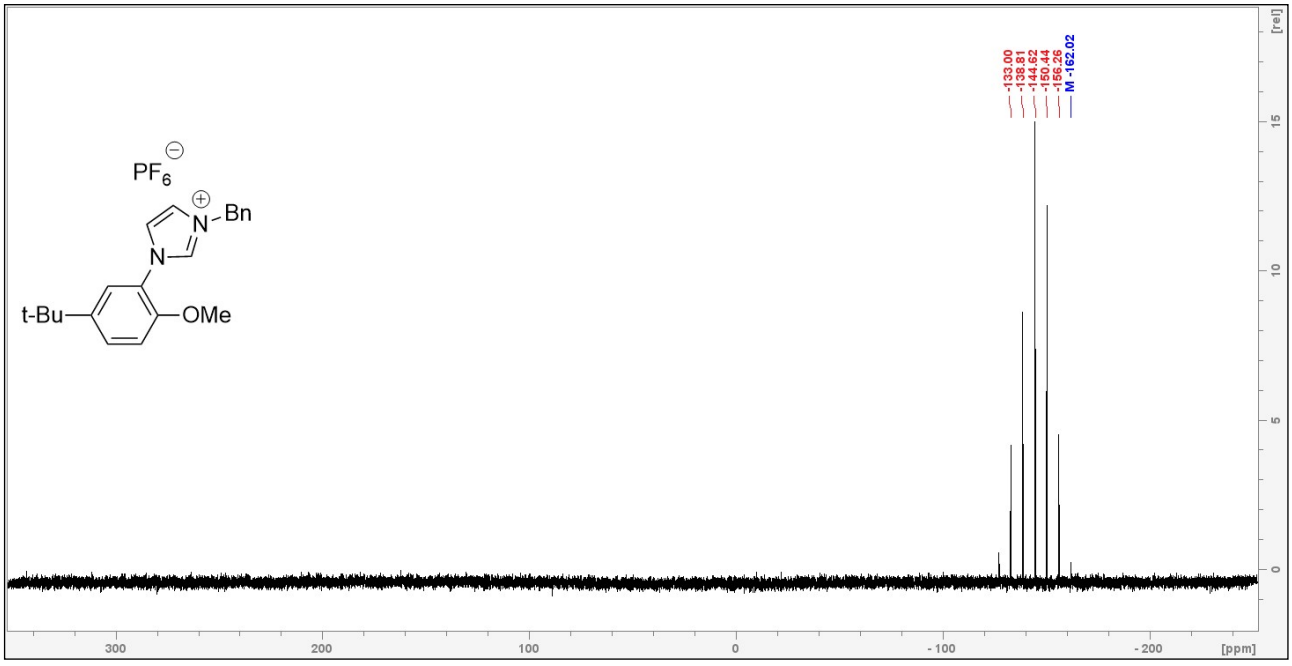

Figure S21. ^{31}P NMR spectra of **Ha^{1}PF$_6$** in CD_3CN.

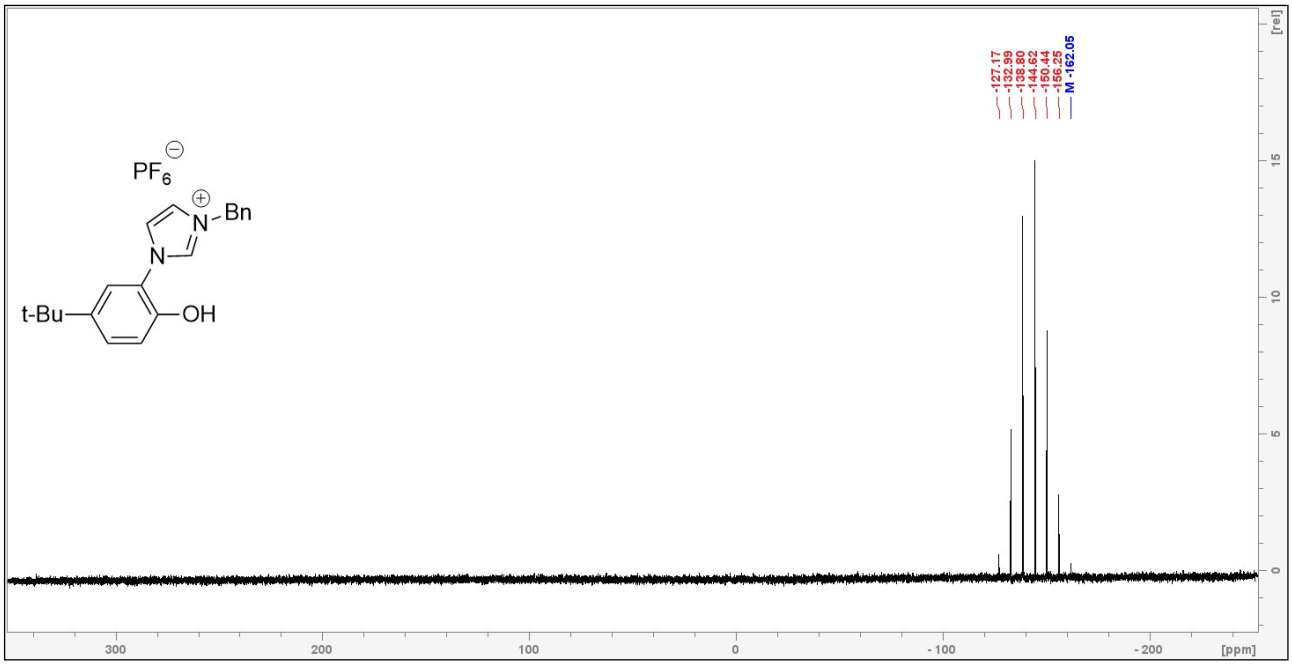

Figure S22. ^{31}P NMR spectra of **H$_2$L^{1}PF$_6$** in CD_3CN.

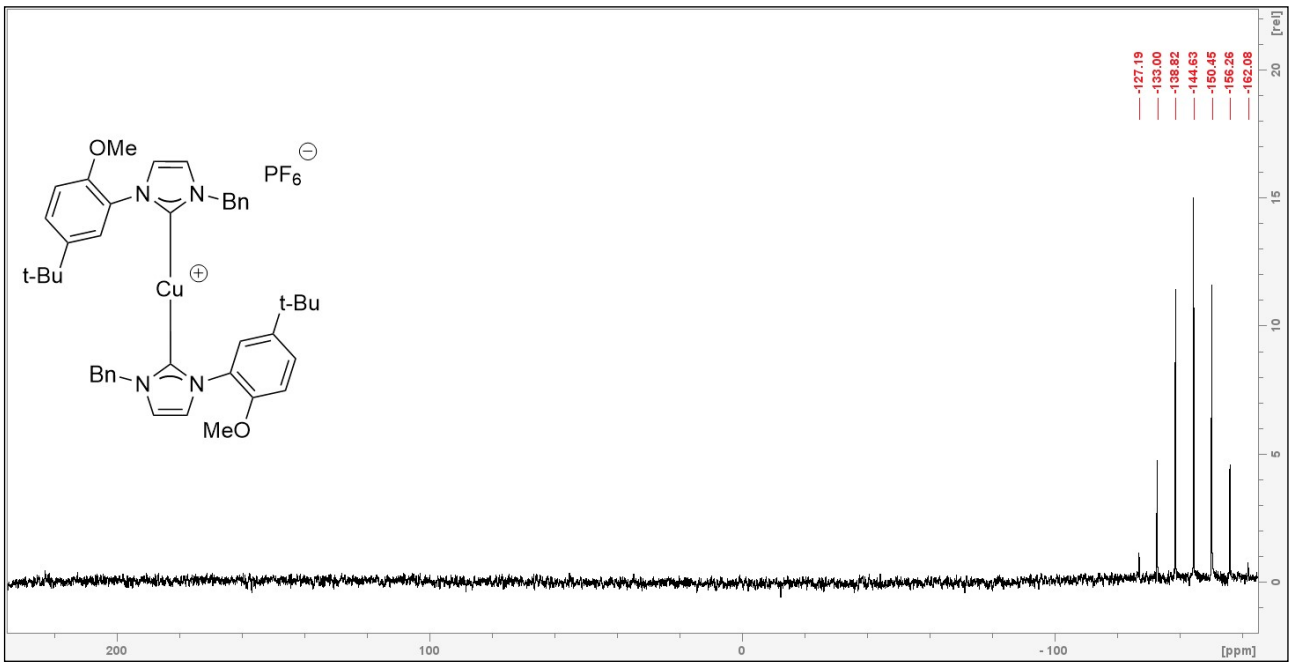

Figure S23. ^{31}P NMR spectra of **[Cu(a^1)$_2$]PF$_6$** in CD_3CN.

4. ^{19}F NMR spectra

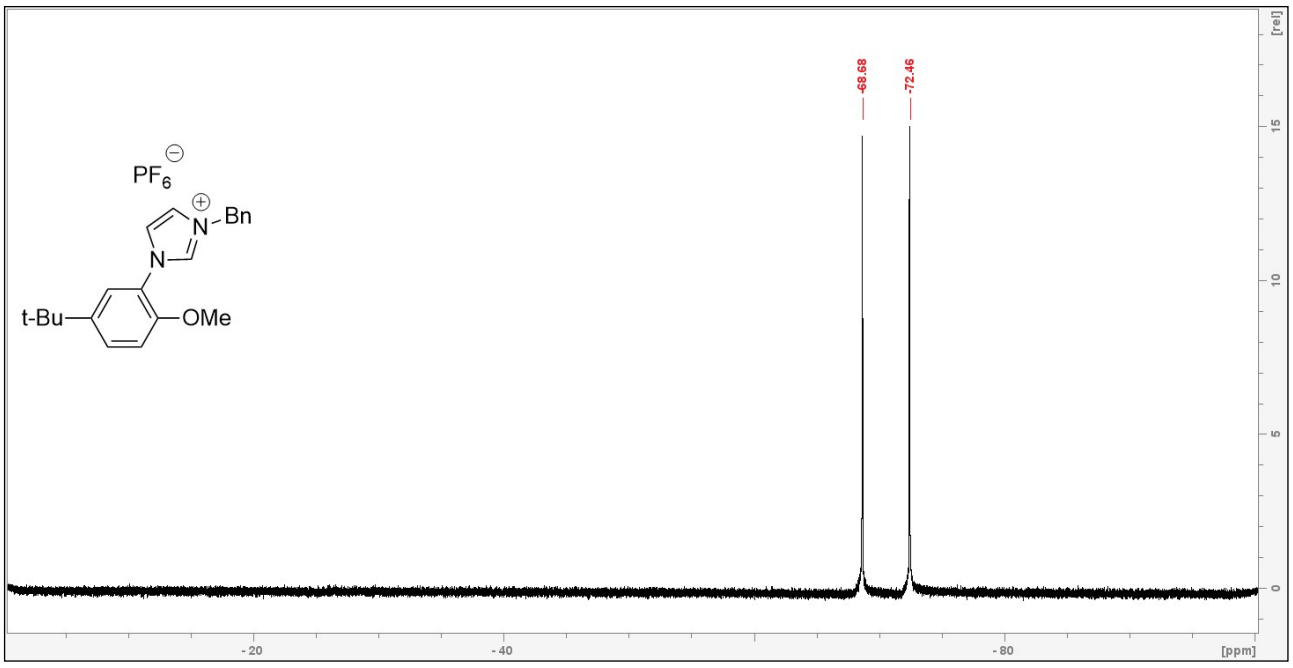

Figure S24. ^{19}F NMR spectra of **Ha^{1}PF$_6$** in CD_3CN.

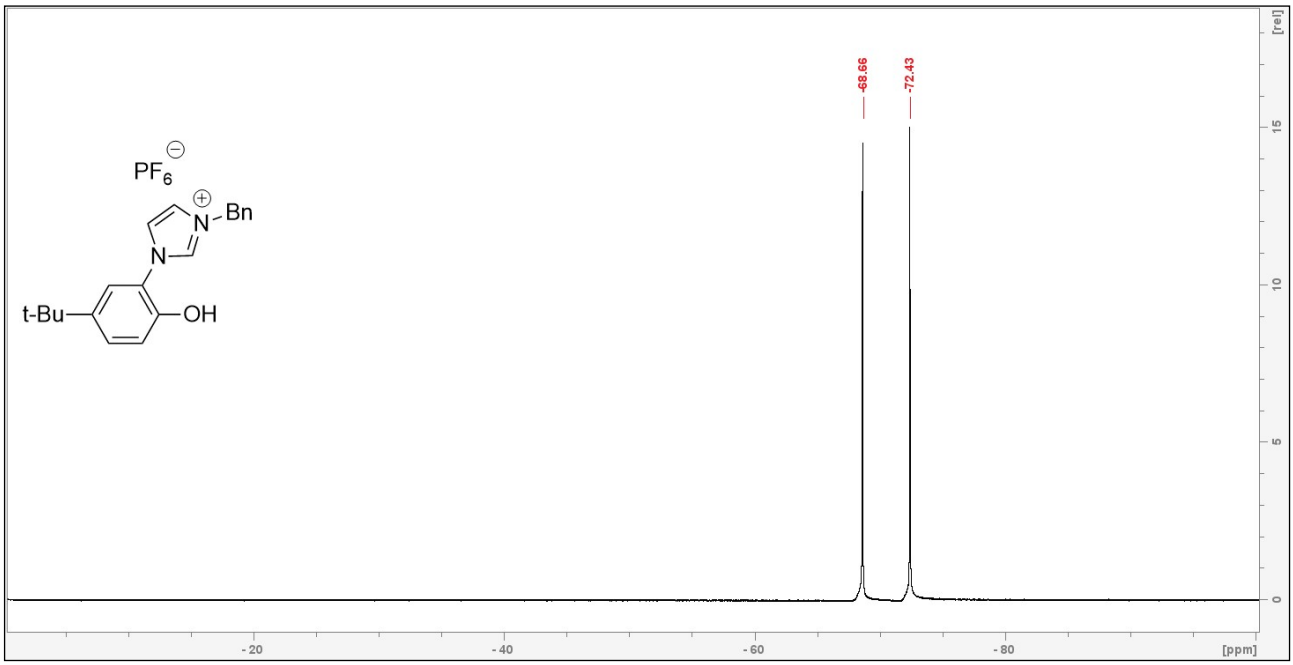

Figure S25. ^{19}F NMR spectra of **H_2L^3Br** in DMSO–d_6.

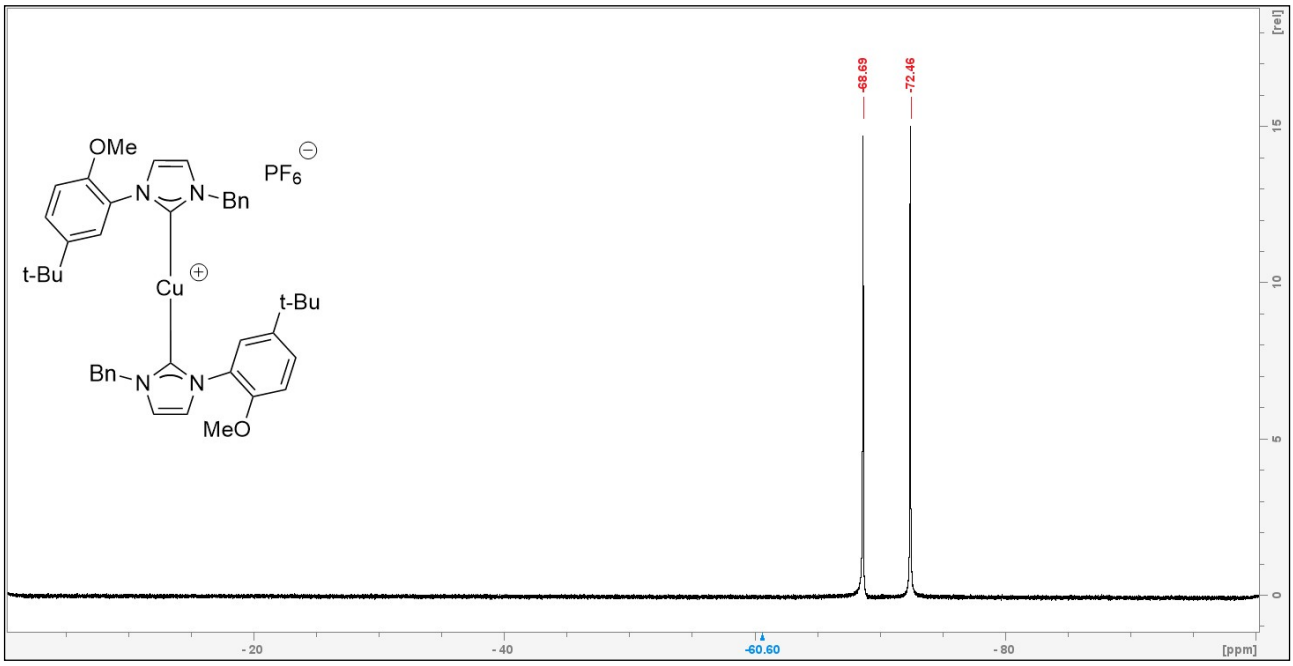

Figure S26. ^{19}F NMR spectra of **$[Cu(a^1)_2]PF_6$** in CD_3CN.

5. 2D NMR spectra

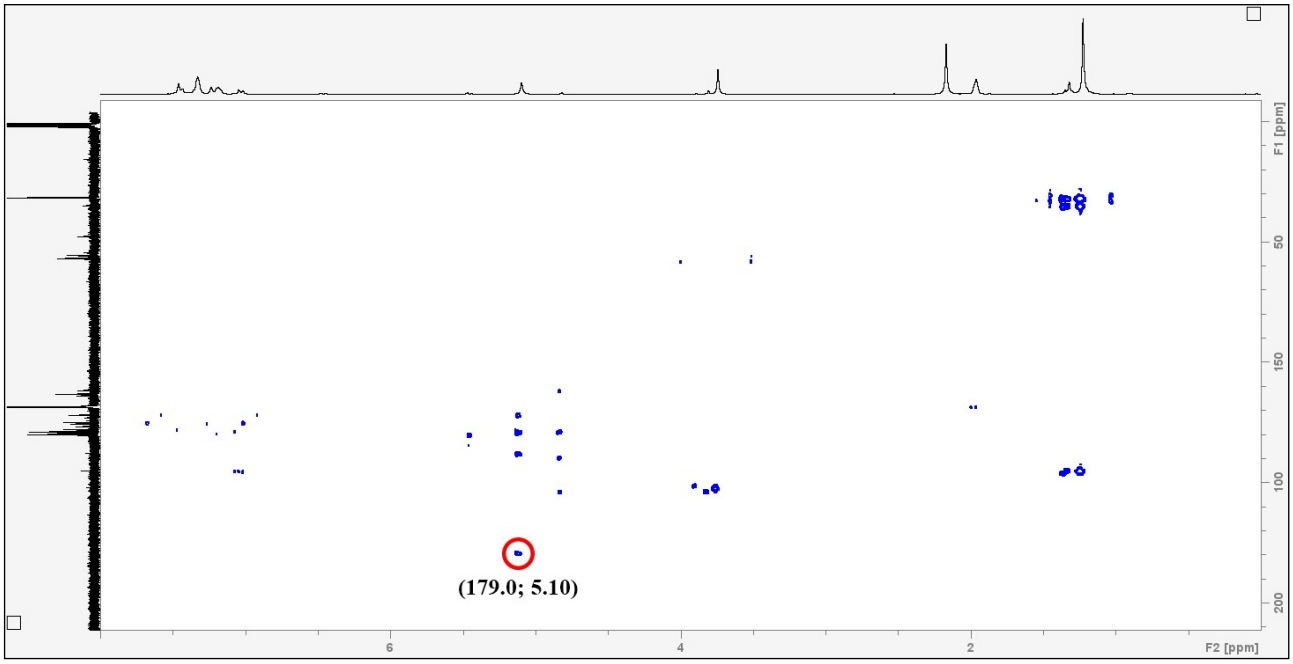

Figure S27. 2D NMR HMBC ^{13}C–^{1}H spectra of **[Cu(a^{1})$_2$]PF$_6$** in CD_3CN.

6. ESI(+)–MS spectra

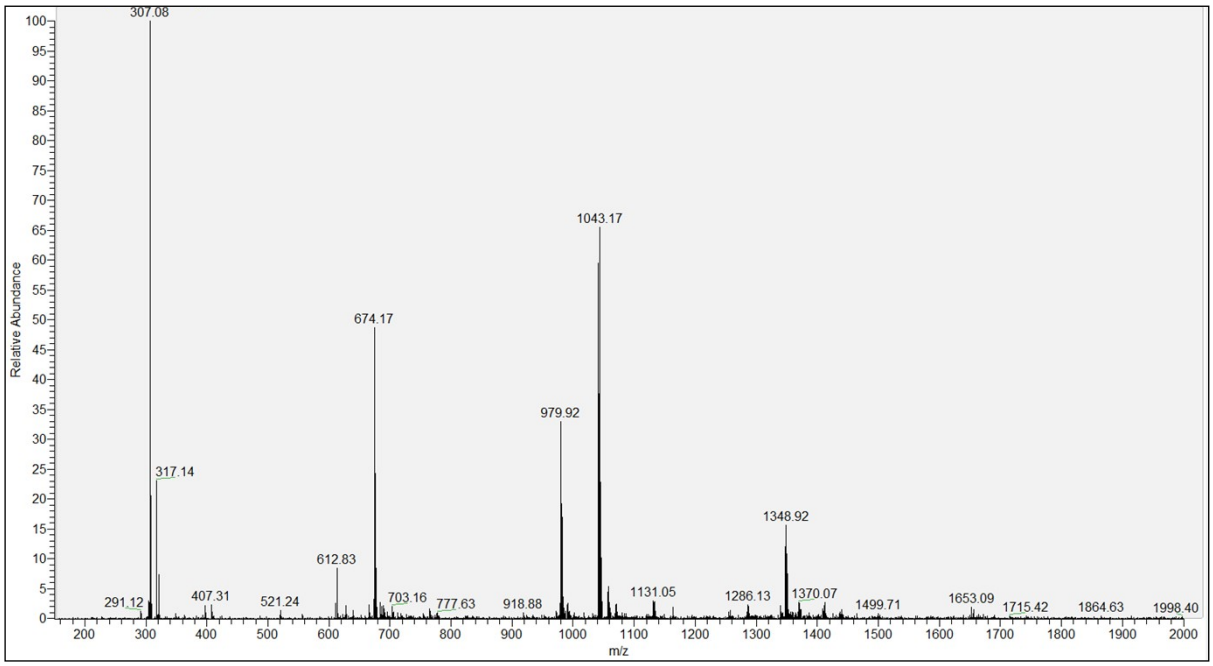

Figure S28. ESI–MS spectra of **[Cu(L^{1})$_2$]**.

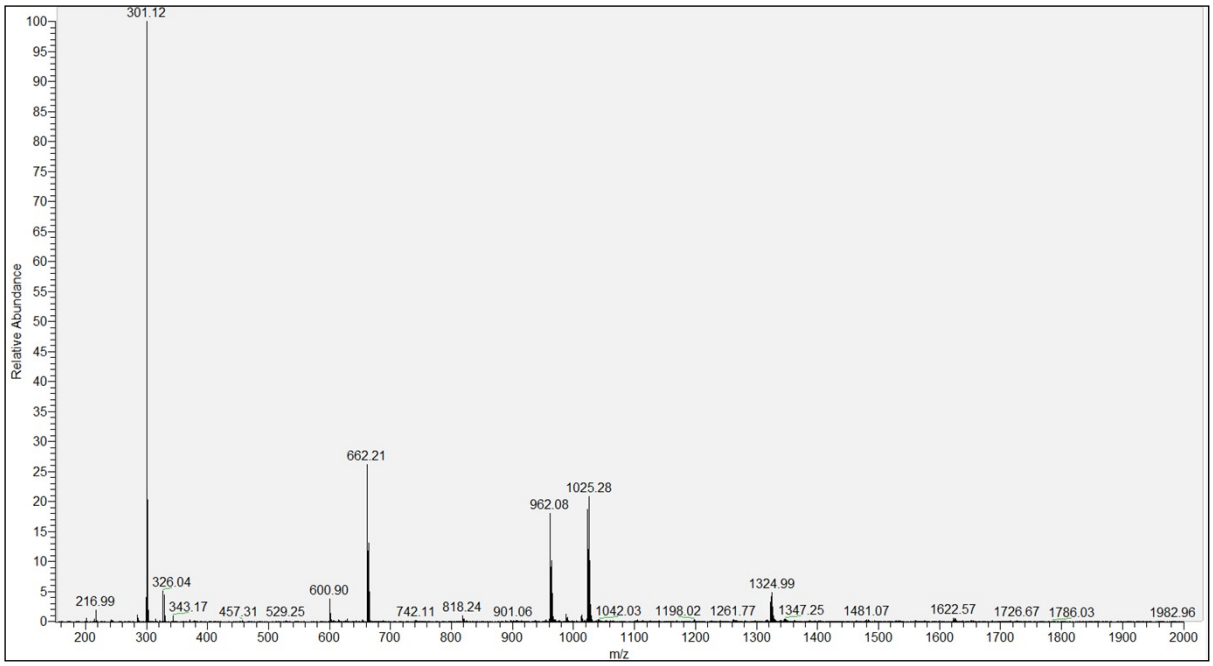

Figure S29. ESI–MS spectra of **[Cu(L^2)$_2$]**.

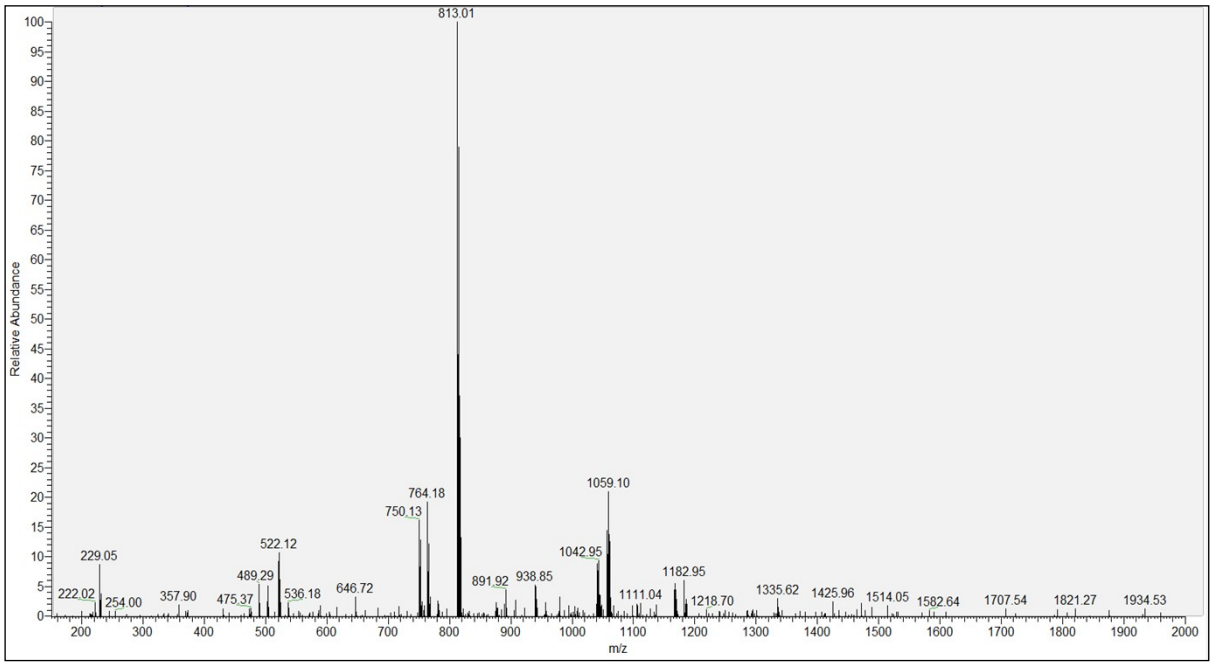

Figure S30. ESI–MS spectra of **[Cu(L^3)$_2$]**.

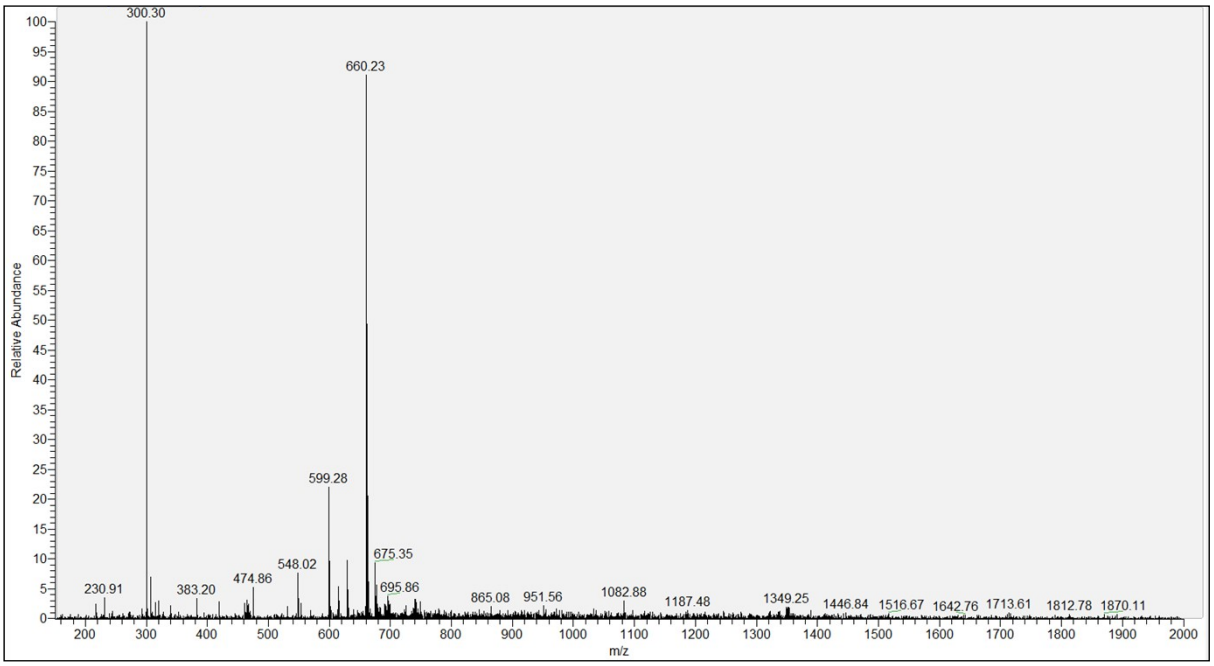

Figure S31. ESI–MS spectra of **[Cu(L^4)]**.

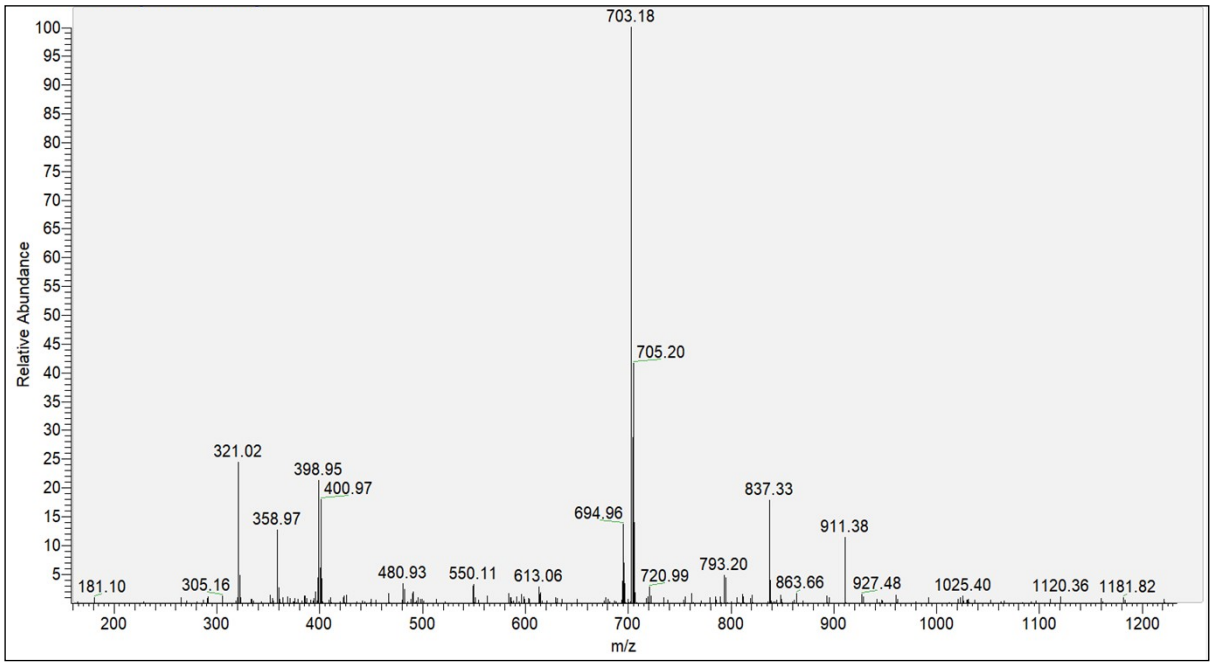

Figure S32. ESI–MS spectra of **[CuBr(a^1)]**.

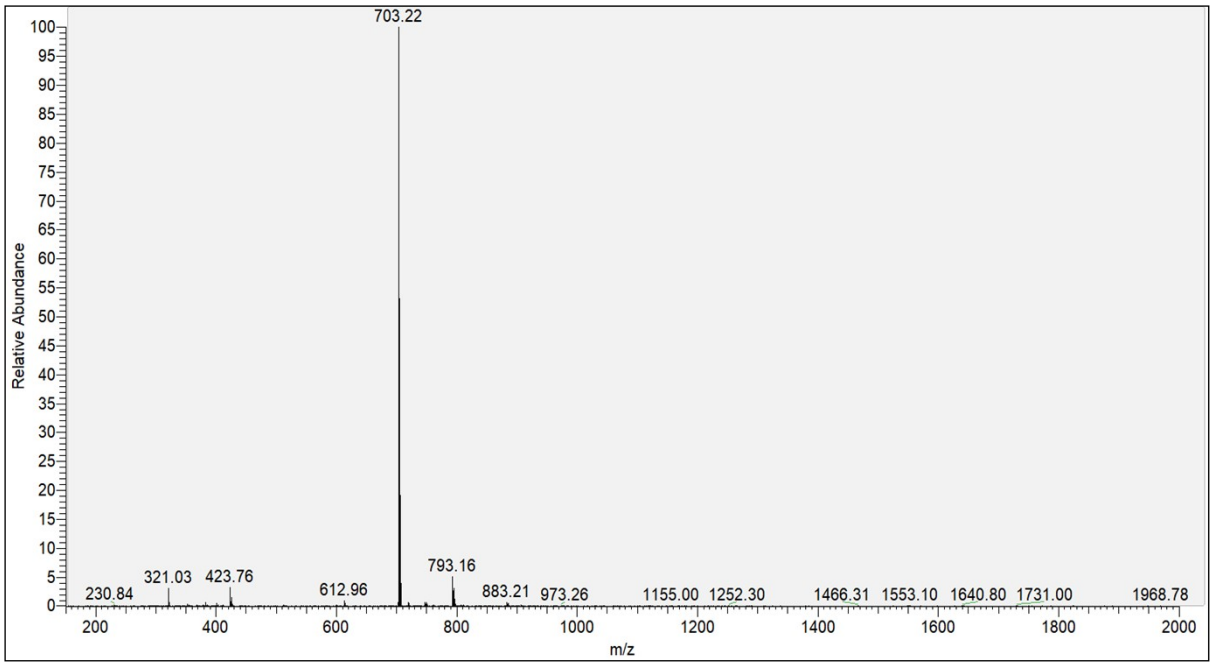

Figure S33. ESI–MS spectra of **[Cu(a^1)$_2$]PF$_6$**.

7. FT-IR spectra

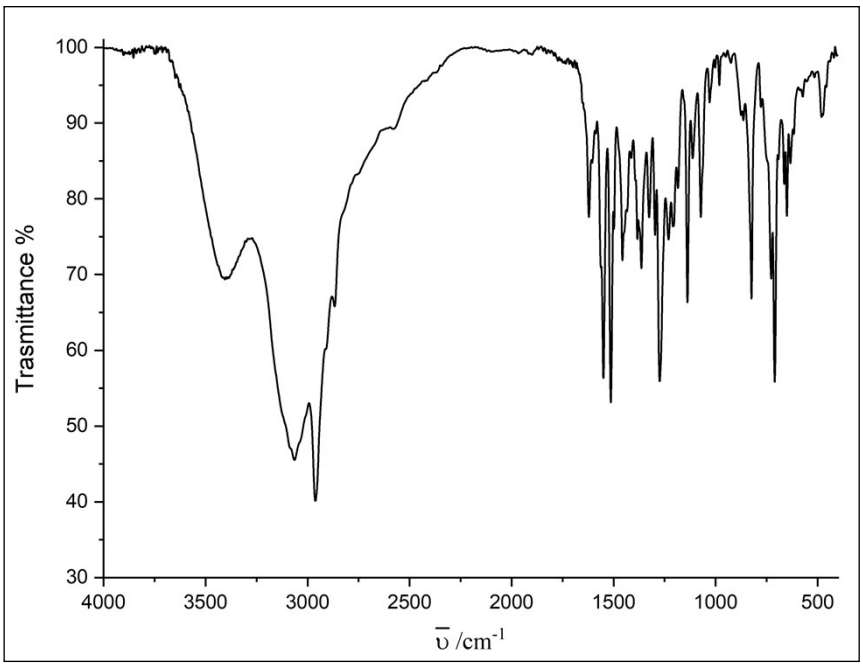

Figure S34. FT-IR spectra of **Ha^{1}Br**.

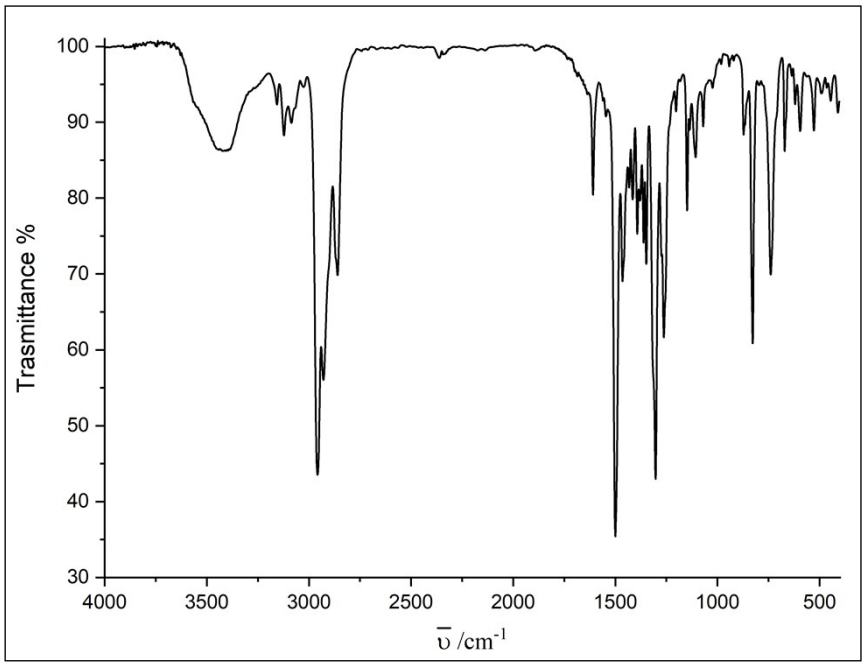

Figure S35. FT-IR spectra of **[Cu(L^1)$_2$]**.

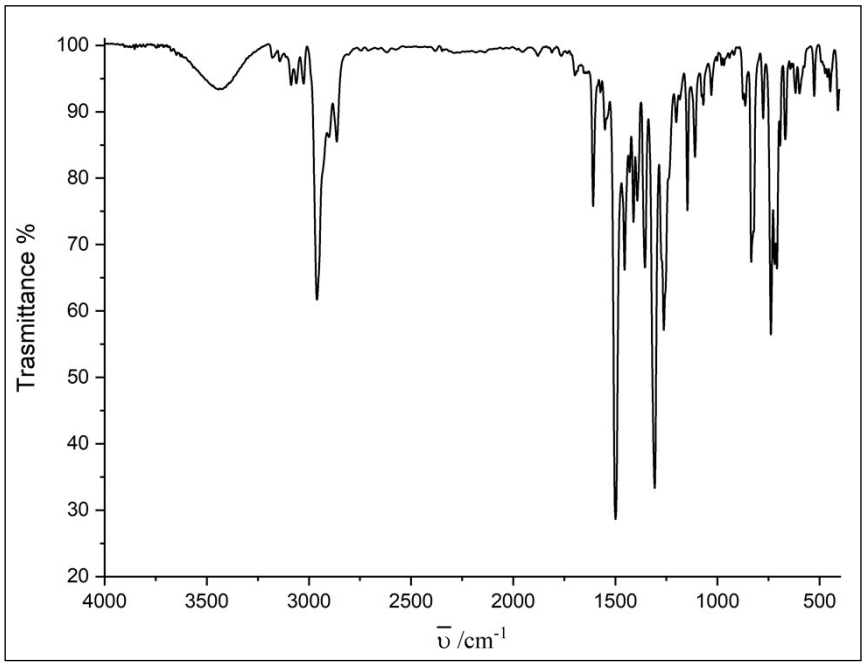

Figure S36. FT-IR spectra of **[Cu(L^2)$_2$]**.

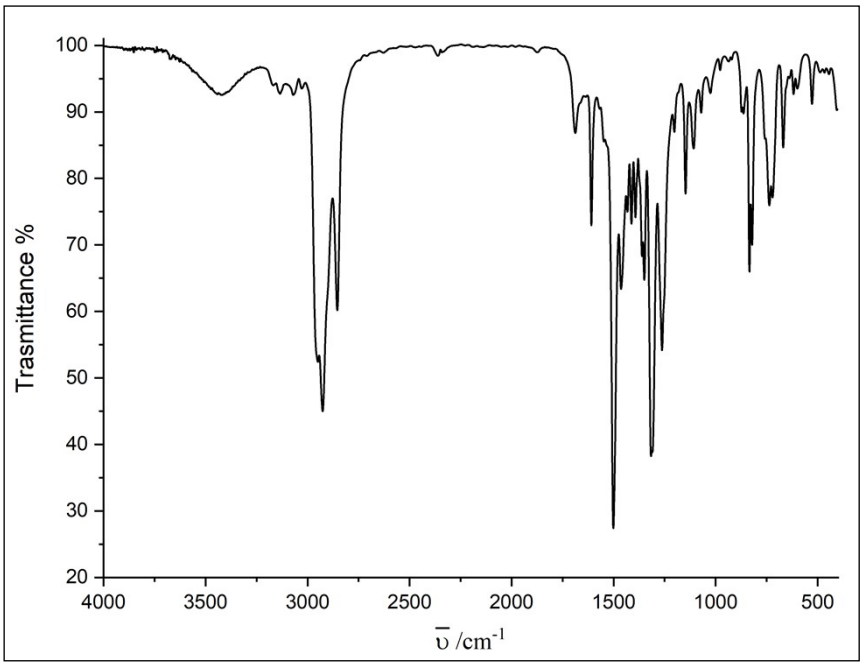

Figure S37. FT-IR spectra of **[Cu(L^3)$_2$]**.

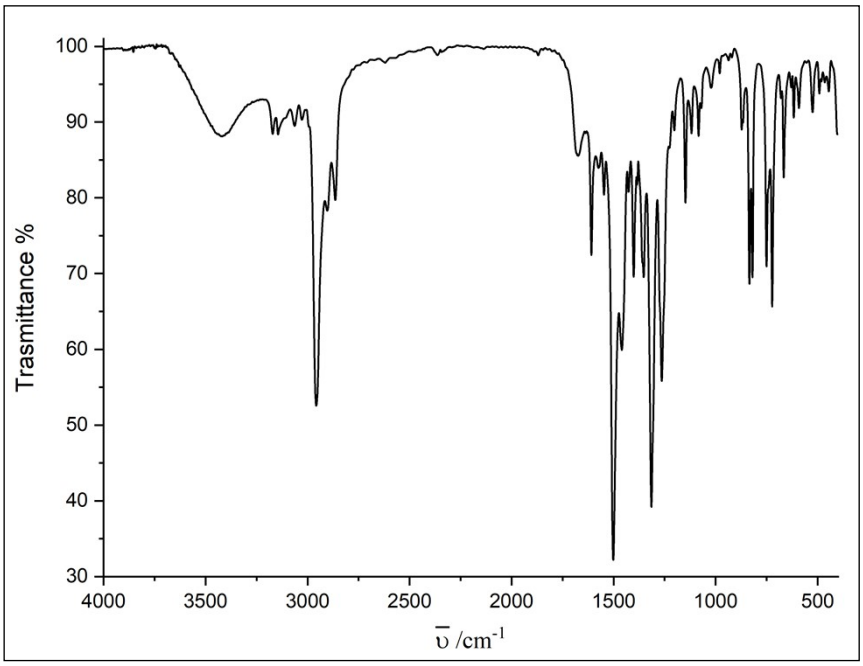

Figure S38. FT-IR spectra of **[Cu(L^4)]**.

8. UV-Vis spectra

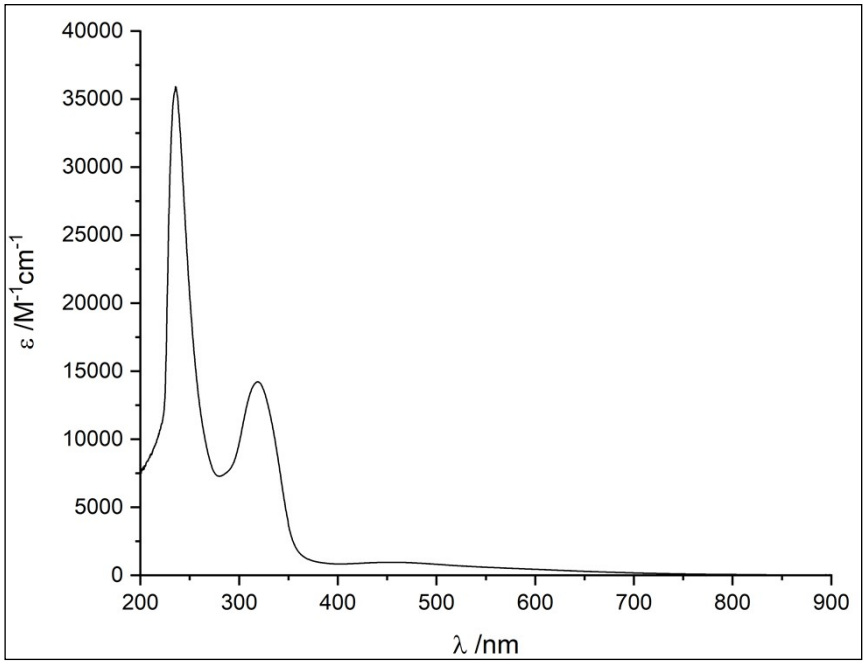

Figure S39. UV-Vis absorption spectra of **[Cu(L^1)$_2$]** in dichloromethane.

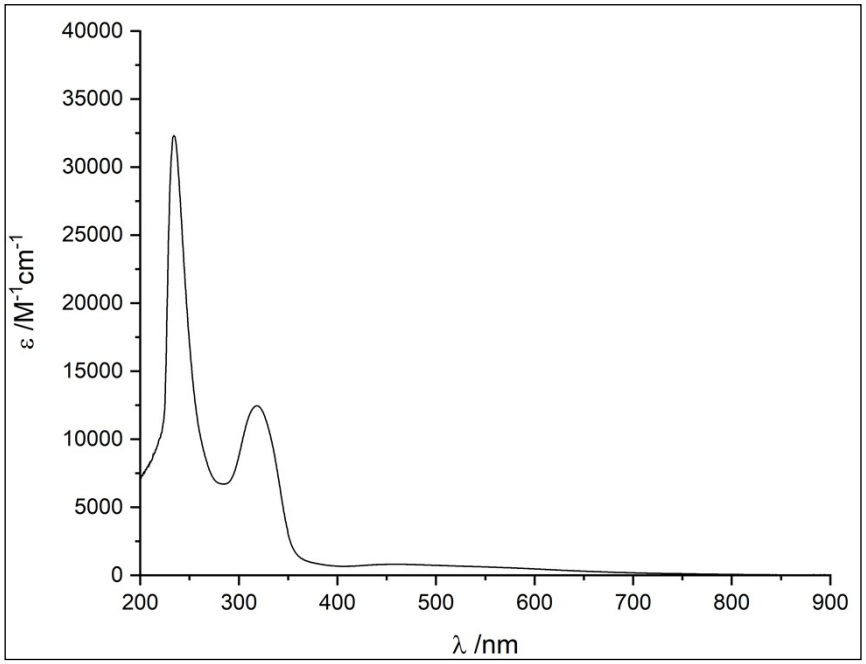

Figure S40. UV-Vis absorption spectra of **[Cu(L^2)$_2$]** in dichloromethane.

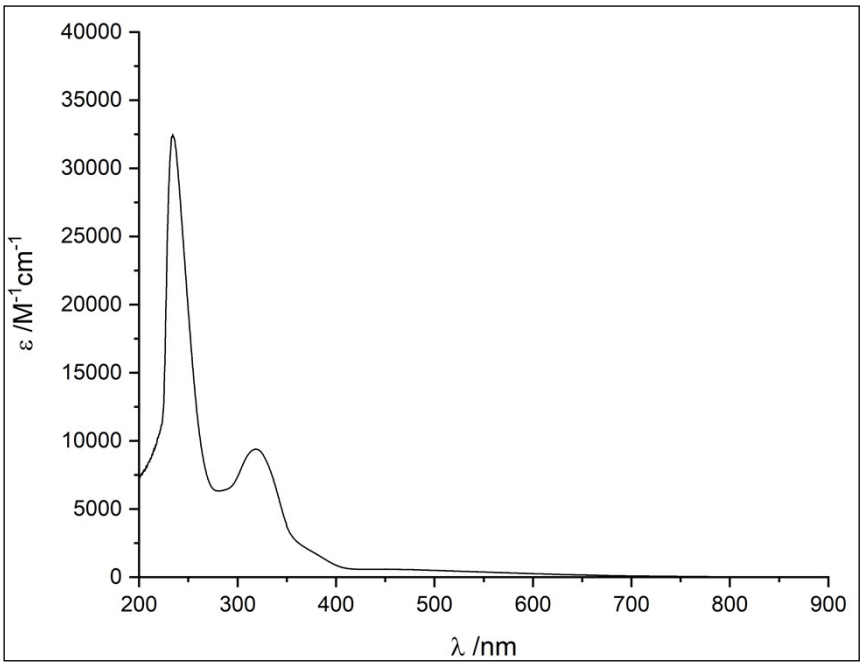

Figure S41. UV-Vis absorption spectra of **[Cu(L^3)$_2$]** in dichloromethane.

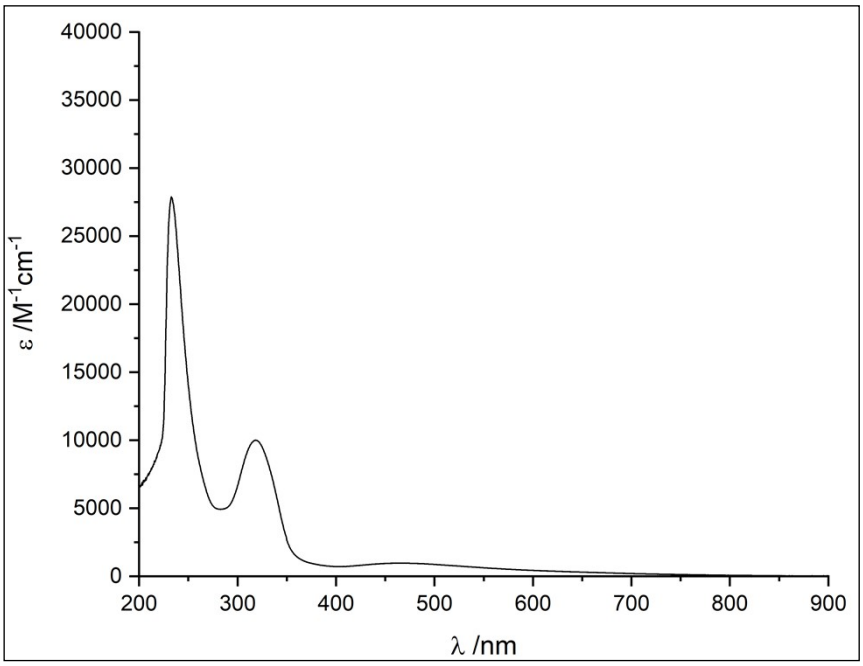

Figure S42. UV-Vis absorption spectra of **[Cu(L^4)]** in dichloromethane.

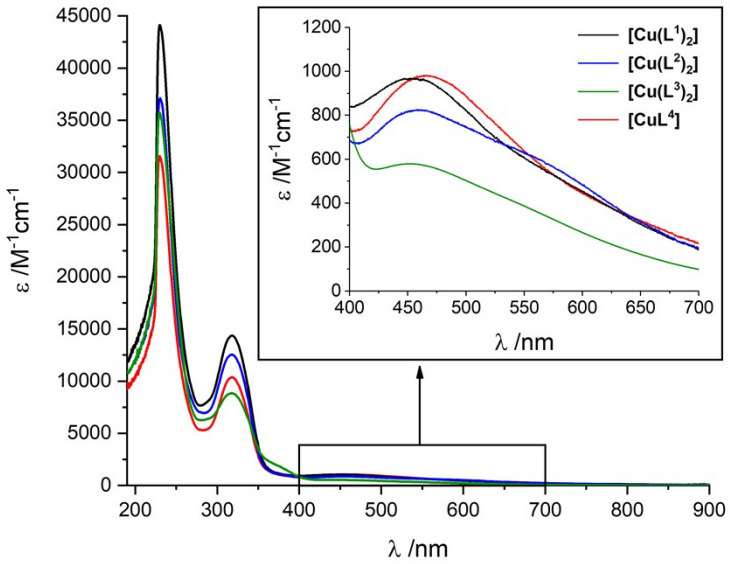

Figure S43. UV-vis. absorption spectra of the reported copper(II) complexes in dichlorometane.

9. SC-XRD data

Table S1: Crystallographic details for complex **[Cu(L^1)$_2$]** and **[CuBr(a^1)]**.

	[Cu(L^1)$_2$]	**[CuBr(a^1)]**
Empirical formula	$C_{40}H_{42}CuN_4O_2$	$C_{21}H_{24}BrCuN_2O$
Formula weight	674.31	463.87
Temperature /K	200(2)	301(2)
Crystal system	monoclinic	monoclinic
Space group	$P2_1$	Cc
a/Å	10.9603(2)	15.9866(3)
b/Å	10.4001(2)	12.9150(3)
c/Å	14.9309(3)	10.0896(2)
α/°	90	90
β/°	98.830(2)	91.323(2)
γ/°	90	90
Volume/Å^3	1681.78(6)	2082.61(7)
Z	2	4
ρ_{calc}g/cm^3	1.332	1.479
μ/mm^{-1}	0.691	3.807
F(000)	710.0	944.0
Crystal size/mm^3	0.18 x 0.17 x 0.15	0.12 x 0.11 x 0.10
Radiation	MoKα (λ = 0.71073)	CuKα (λ = 1.54184)
2Θ range for data collection/°	3.76 to 51.354	12.344 to 144.242
Index ranges	-13 ≤ h ≤ 13, -12 ≤ k ≤ 12, -18 ≤ l ≤ 18	-19 ≤ h ≤ 19, -15 ≤ k ≤ 15, -12 ≤ l ≤ 12
Reflections collected	73871	27598
Independent reflections	6396 [R_{int} = 0.0665, R_{sigma} = 0.0260]	4015 [R_{int} = 0.0427, R_{sigma} = 0.0221]
Data/restraints/parameters	6396/1/430	4015/2/239
Goodness-of-fit on F^2	1.035	1.000
Final R indexes [I>=2σ (I)]	R_1 = 0.0259, wR_2 = 0.0655	R_1 = 0.0386, wR_2 = 0.1158
Final R indexes [all data]	R_1 = 0.0271, wR_2 = 0.0666	R_1 = 0.0404, wR_2 = 0.1189
Largest diff. peak/hole / e Å^{-3}	0.18/-0.33	0.69/-0.37
CCDC number	2371863	2371864

$R_1 = (\Sigma||F_o| - |F_c||/\Sigma|F_o|)$; $wR_2 = \{\Sigma[w(F_o^2 - F_c^2)^2]/\Sigma[w(F_o^2)^2]\}^{1/2}$; GOF $=\Sigma[w(F_o^2-F_c^2)^2]/(n-p)\}^{½}$ where n is the number of data and p is the number of parameters refined.

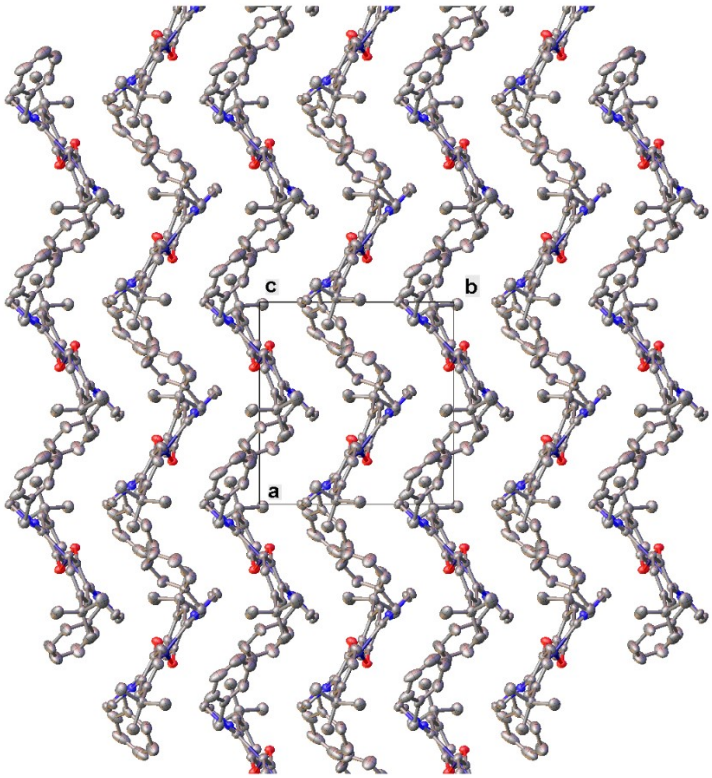

Figure S44. ORTEP representation of the crystal packing of complex **[Cu(L^1)$_2$]** (view along *c* axis).

10. Catalysis

The yield determination of the catalytic tests was conducted registering the ^{1}H NMR spectra of the reaction mixture in $CDCl_3$, after addition of 0.5 equivalents of an 2,5-dimethylfuran as internal standard. Using the benchmark substrate N-ethylaniline, the yields of *N*-ethylformaniline and *N*-methyl-*N*-ethylaniline were calculated using the integral of the signals at 8.35 and 2.90 ppm respectively (Fig. S45). The unreacted *N*-ethylaniline amount was estimated from the integral of the quartet at 3.15 ppm. The residual silane amount was instead calculated on the Si-H signal integral, at 4.20 ppm for the phenylsilane. The integrals values were referred to the CH proton signal of the internal standard 2,5-dimethylfuran, to have accurate estimations. In all the catalytic tests reported, no loss of matter was observed.

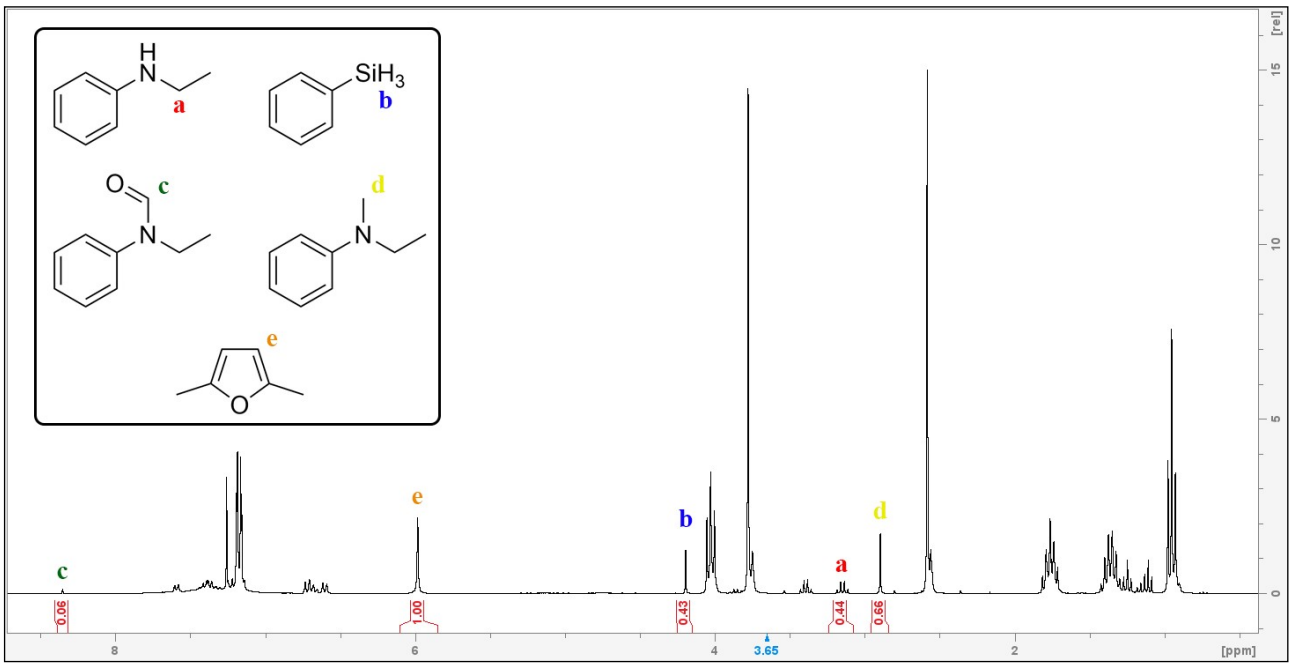

Figure S45. ^{1}H NMR spectrum in $CDCl_3$ of a generic catalytic reaction using *N*-ethylaniline as substrate, phenylsilane as reducing agent, and [BMMIM][NTf_2] as solvent.

^{1}H NMR chemical shifts for the quantification of the compounds:

***N*-ethylaniline (1a)** [1] ^{1}H NMR (400 MHz, $CDCl_3$): δ = 7.24–7.10 (m, 2H), 6.76–6.64 (m, 1H), 6.64–6.52 (m, 2H), 3.49 (s, 1H), 3.13 (q, *J* = 7.1 Hz, 2H), 1.23 (t, *J* = 7.1 Hz, 3H) ppm.

***N*-ethylformanilide (3a)** [2] ^{1}H NMR (500 MHz, $CDCl_3$): δ = 8.35 (s, 1H), 7.40 (t, J = 8.0 Hz, 2H), 7.29 (t, *J* = 7.5 Hz, 1H), 7.16 (d, *J* = 7.5 Hz, 2H), 3.85 (q, *J* = 7.0 Hz, 2H), 1.15 (t, *J* = 7.0 Hz, 3H) ppm.

***N*-methyl-*N*-ethylaniline (2a)** [3] ^{1}H NMR (600 MHz, $CDCl_3$): δ = 7.22 (t, *J* = 7.8 Hz, 2H), 6.72 (d, *J* = 8.3 Hz, 2H), 6.68 (t, *J* = 7.2 Hz, 1H), 3.39 (q, *J* = 7.1 Hz, 2H), 2.89 (s, 3H), 1.11 (t, *J* = 7.1 Hz, 3H) ppm.

***N*-methylaniline (1b)** [1] ^{1}H NMR (400 MHz, $CDCl_3$): δ = 7.39–7.02 (m, 2H), 6.70 (tt, *J* = 7.3, 1.1 Hz, 1H), 6.64–6.55 (m, 2H), 3.66 (s, 1H), 2.81 (s, 3H) ppm.

***N*-methylformanilide (3b)** [2] ^{1}H NMR (400 MHz, $CDCl_3$): δ = 8.52 (s, 1H), 7.46 (t, *J* = 7.6 Hz, 2H), 7.32 (t, *J* = 7.6 Hz, 1H), 7.21 (d, *J* = 7.2 Hz, 2H), 3.36 (s, 3H) ppm.

***N,N*-dimethyl-aniline (2b)** [3] ^{1}H NMR (600 MHz, $CDCl_3$): δ = 7.27 (t, *J* = 7.7 Hz, 2H), 6.76 (dd, *J* = 17.4, 7.9 Hz, 3H), 2.97 (s, 6H) ppm.

4-methoxy-*N*-methylaniline (1c) [1] ^{1}H NMR (400 MHz, $CDCl_3$): δ = 6.80 (d, *J* = 8.9 Hz, 2H), 6.58 (d, *J* = 8.9 Hz, 2H), 3.75 (s, 3H), 2.80 (s, 3H) ppm.

***N*-(4-methoxyphenyl)-*N*-methylformamide (3c)** [4] ^{1}H NMR (400 MHz, $CDCl_3$): δ = 8.34 (s, 1H), 7.10 (d, *J* = 9.2 Hz, 2H), 6.93 (d, *J* = 8.0 Hz, 2H), 3.82 (s, 3H), 3.27 (s, 3H) ppm.

4,4-*N,N*-dimethylaminoanisole (2c) [5] ^{1}H NMR (400 MHz, $CDCl_3$): δ = 6.84 (d, *J* = 8.6 Hz, 2H), 6.75 (d, *J* = 8.9 Hz, 2H), 2.86 (s, 6H), 3.76 (s, 3H) ppm.

Dibenzylamine (1d) [6] ^{1}H NMR (500 MHz, $CDCl_3$): δ = 7.26–7.22 (m, 4H), 7.19–7.14 (m, 4H), 3.72 (s, 4H) ppm.

***N,N*-dibenzylformamide (3d)** [7] ^{1}H NMR (400 MHz, $CDCl_3$): δ = 8.35 (s, 1H), 7.35 – 7.22 (m, 6H), 7.14 (m, 4H), 4.36 (s, 2H), 4.19 (s, 2H) ppm.

***N,N*-dibenzyl-methylamine (2d)** [8] ^{1}H NMR (400 MHz, $CDCl_3$): δ = 7.37-7.29 (m, 8H), 7.25-7.21 (m, 2H), 3.51 (s, 4H), 2.18 (s, 3H) ppm.

Table S2

Preliminary catalytic experiments in the N-methylation and N-formylation of *N*-ethylaniline with CO_2 and phenylsilane.

Entry	Catalyst	Solvent	p / bar	t /h	Conv. /% [a]	**2a** /% [a]	**3a** /% [a]
1	-	Acetonitrile	5	5	0	0	0
2	H_2L^1Br	Acetonitrile	5	5	0	0	0
3	$Cu(OAc)_2 \cdot H_2O$	Acetonitrile	5	5	0	0	0
4	$[Cu(L^1)_2]$	Acetonitrile	5	5	87	8	79
5	$[Cu(L^1)_2]$	Acetonitrile	3	5	65	7	58
6	$[Cu(L^1)_2]$	Toluene	3	5	0	0	0
7	$[Cu(L^1)_2]$	Methanol	3	5	0	0	0
8	$[Cu(L^1)_2]$	Acetone	3	5	12	2	10
9	$[Cu(L^1)_2]$	DMF	3	5	>99	23	77
10	$[Cu(L^1)_2]$	[BMMIM][NTf_2]	3	5	>99	30	70
11	-	[BMMIM][NTf_2]	3	16	0	0	0

Reaction conditions: *N*-ethylaniline 0.40 mmol, $PhSiH_3$ (3 eq), catalyst load 1 mol%, 40 °C, 19 h, in 1 mL of solvent.

[a] Yield determined by ^1H NMR using 2,5-dimethylfuran as an internal standard.

Table S3

Catalytic experiments in the N-methylation and N-formylation of *N*-ethylaniline with CO_2 and phenylsilane with different Cu(II) complexes..

Entry	Catalyst	Time /h	Conv. /% [a]	**2a** /% [a]	**3a** /% [a]
1	**[Cu(L^1)$_2$]**	1	5	3	2
2	**[Cu(L^1)$_2$]**	3	21	15	6
3	**[Cu(L^1)$_2$]**	5	35	24	11
4	**[Cu(L^1)$_2$]**	7	43	29	14
5	**[Cu(L^1)$_2$]**	24	84	62	22
6	**[Cu(L^1)$_2$]**	30	89	64	25
7[b]	**[Cu(L^1)$_2$]**	30 + 16	100	75	25
8	**[Cu(L^2)$_2$]**	1	6	5	1
9	**[Cu(L^2)$_2$]**	3	34	24	10
10	**[Cu(L^2)$_2$]**	5	65	49	16
11	**[Cu(L^2)$_2$]**	7	84	64	20
12	**[Cu(L^2)$_2$]**	24	100	81	19
13	**[Cu(L^3)$_2$]**	1	5	3	2
14	**[Cu(L^3)$_2$]**	3	14	9	5
15	**[Cu(L^3)$_2$]**	5	19	12	7
16	**[Cu(L^3)$_2$]**	7	22	15	7
17	**[Cu(L^3)$_2$]**	24	29	15	14
18	**[Cu(L^4)]**	1	1	1	0
19	**[Cu(L^4)]**	3	9	7	2
20	**[Cu(L^4)]**	5	17	14	3
21	**[Cu(L^4)]**	7	19	15	5
22	**[Cu(L^4)]**	24	20	15	5
23[c]	**[Cu(L^2)$_2$]**	1	21	19	2
24[c]	**[Cu(L^2)$_2$]**	3	41	37	4
25[c]	**[Cu(L^2)$_2$]**	5	48	43	5
26[C]	**[Cu(L^2)$_2$]**	24	68	59	9

Reaction conditions: *N*-ethylaniline 0.40 mmol, $PhSiH_3$ (3 eq), catalyst load 1 mol%, p(CO_2) = 1 bar (balloon), 60 °C, in 1 mL of [BMMIM][NTf_2]. [a] Yield determined by ^{1}H NMR using 2,5-dimethylfuran as an internal standard. [b] Addition of 3 eq of phenylsilane. [c] T = 80 °C.

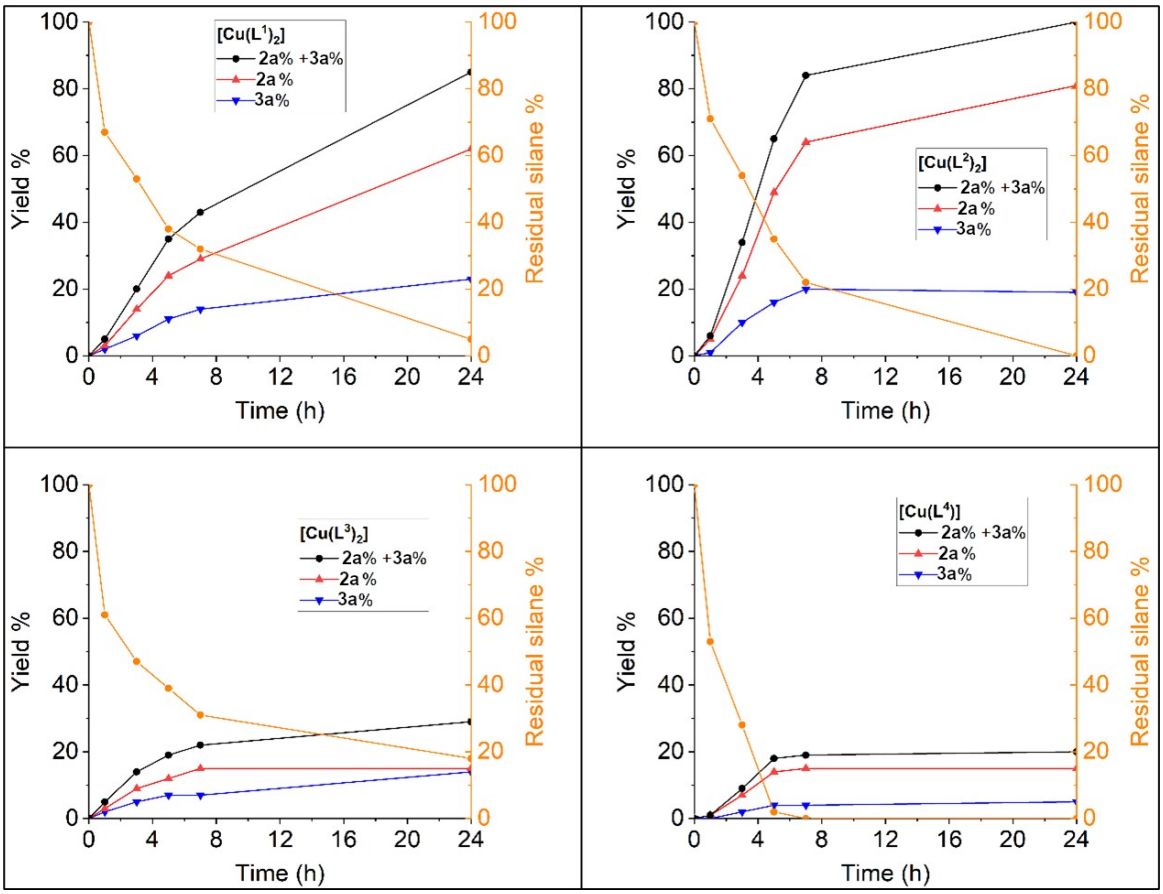

Figure S46a. Yield of *N*-methyl-*N*-ethylaniline (**2a**), N-ethylformanilide (**3a**), sum of the yields and residual phenylsilane against time for the reaction involving the four Cu(II) complexes (data of table S3). *N*-ethylaniline 0.40 mmol, $PhSiH_3$ (3 eq), catalyst load 1 mol%, $p(CO_2)$ = 1 bar, 60 °C.

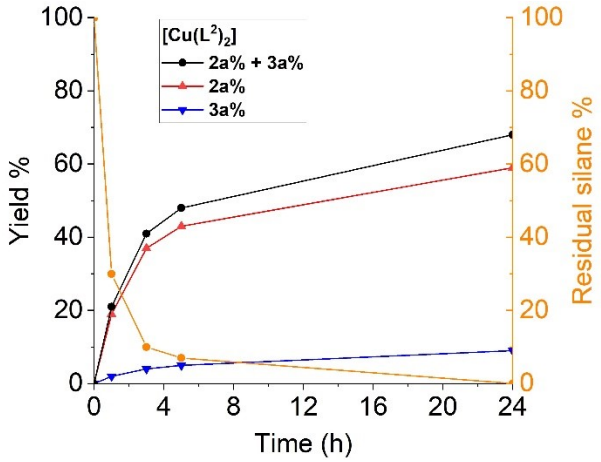

Figure S46b. Yield of *N*-methyl-*N*-ethylaniline (**2a**), N-ethylformanilide (**3a**), sum of the yields and residual phenylsilane against time for the reaction involving **[Cu(L^2)$_2$]** (data of table S3). *N*-ethylaniline 0.40 mmol, $PhSiH_3$ (3 eq), catalyst load 1 mol%, $p(CO_2)$ = 1 bar, 80 °C.

11. Stoichiometric reactions NMR spectra

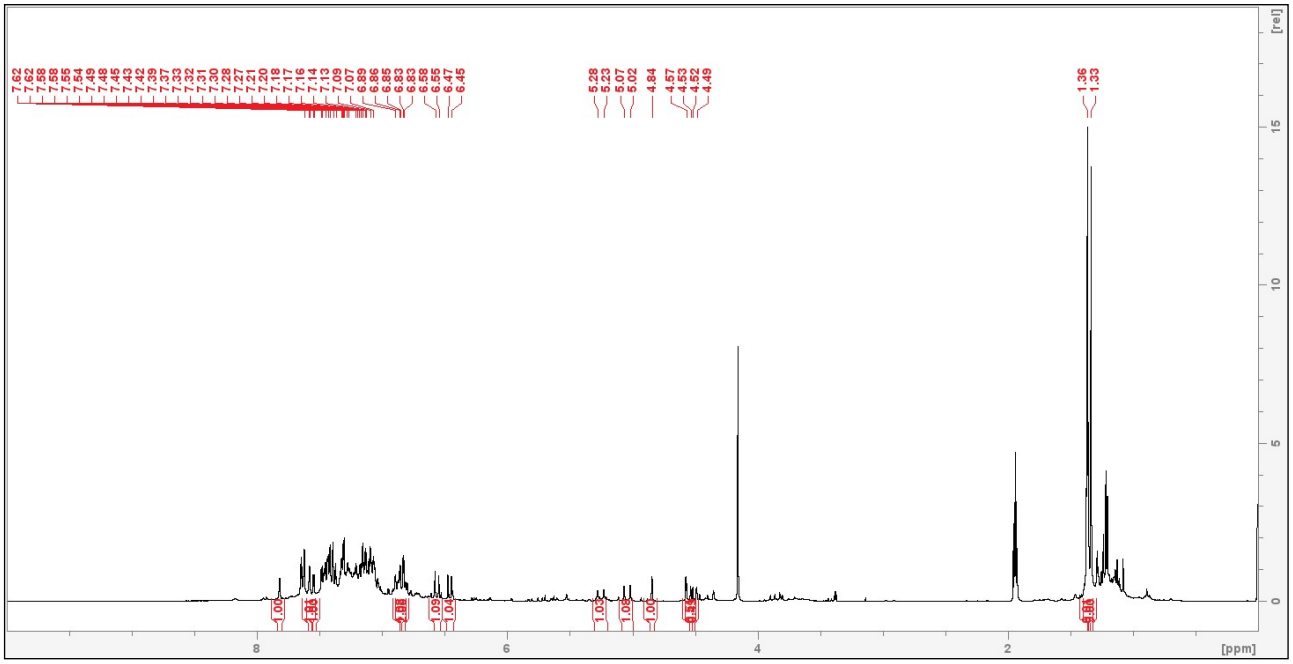

Figure S47. ^{1}H NMR spectra of the reaction between **[Cu(L^{1})$_2$]** and $PhSiH_3$, in CD_3CN.

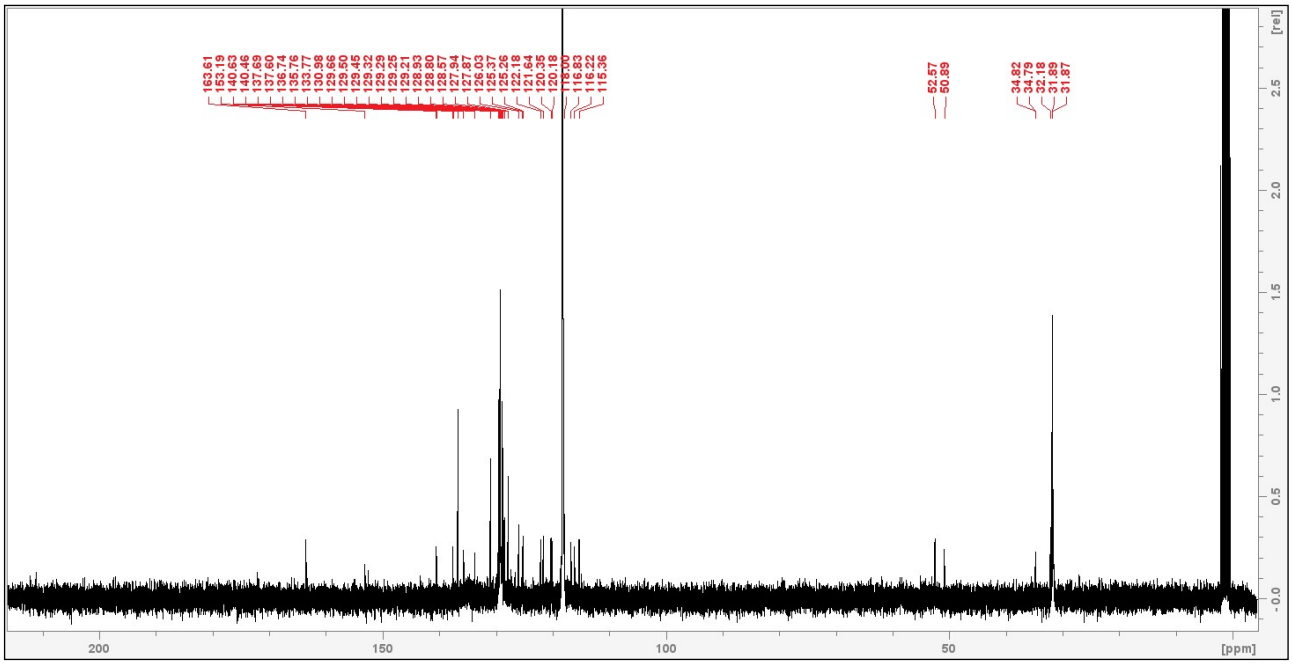

Figure S48. ^{13}C NMR spectra of the reaction between **[Cu(L^{1})$_2$]** and $PhSiH_3$, in CD_3CN.

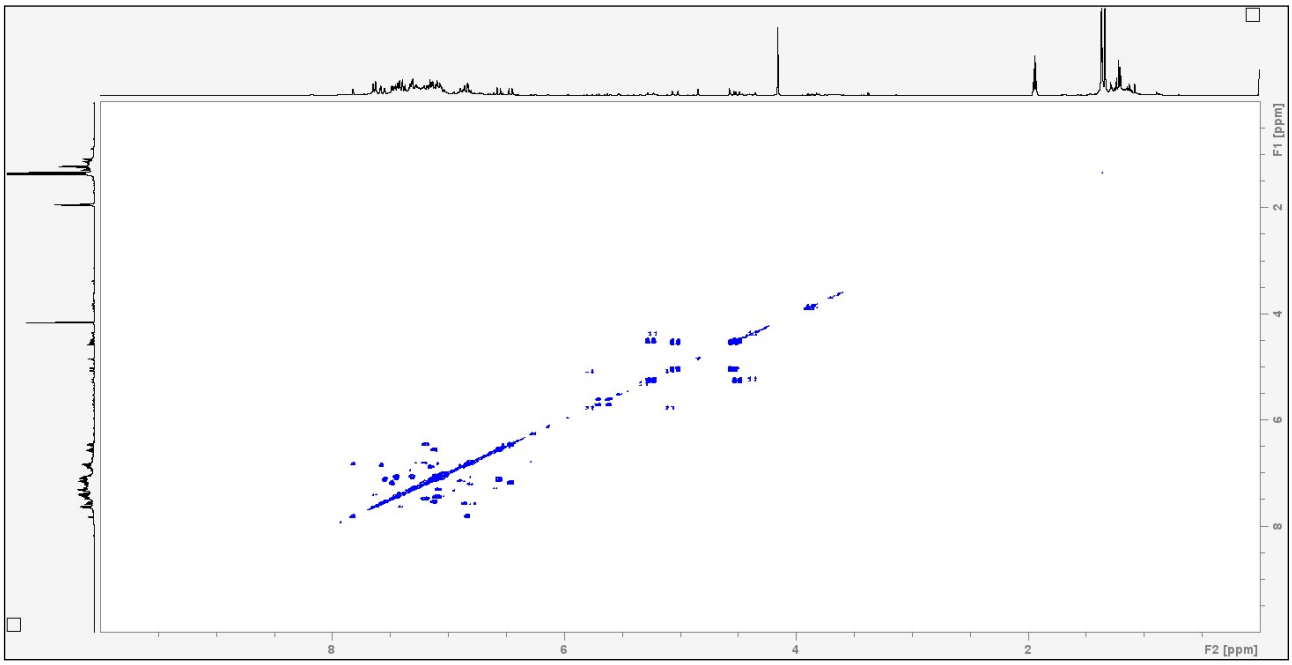

Figure S49. 2D NMR COSY ^{1}H–^{1}H spectra of the reaction between **[Cu(L^{1})$_2$]** and $PhSiH_3$, in CD_3CN.

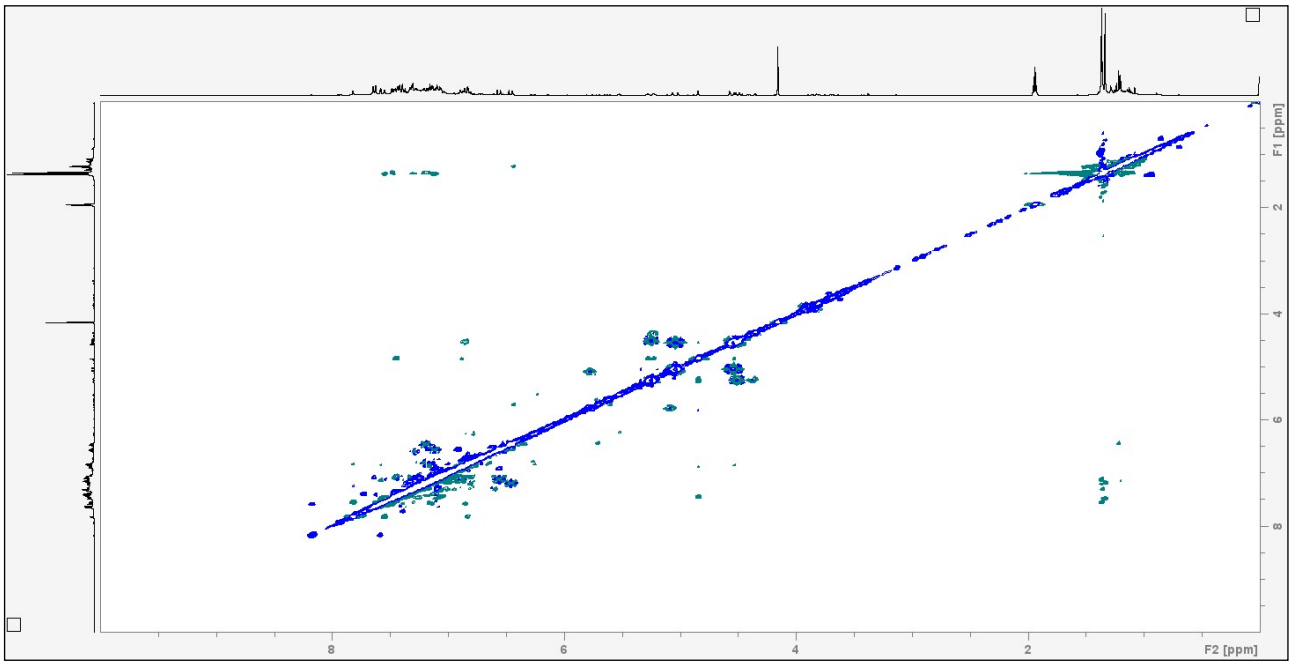

Figure S50. 2D NMR NOE ^{1}H–^{1}H spectra of the reaction between **[Cu(L^{1})$_2$]** and $PhSiH_3$, in CD_3CN.

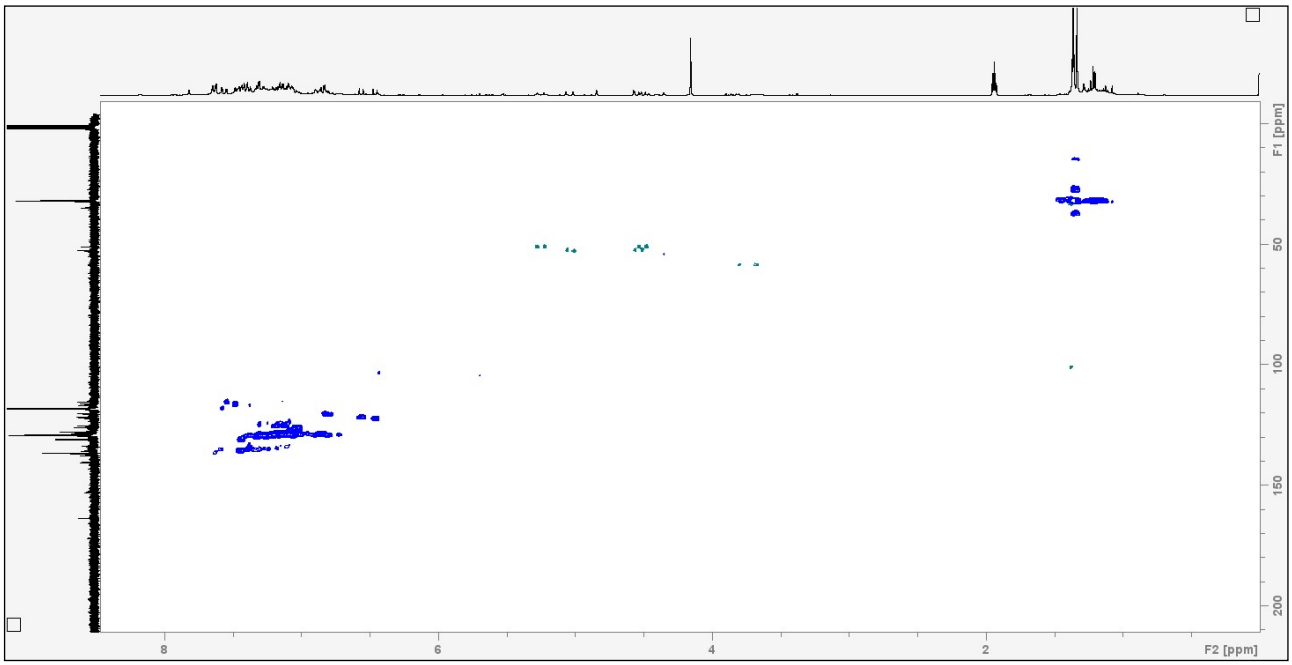

Figure S51. 2D NMR HSQC INEPT ^{13}C–^{1}H spectra of the reaction between **[Cu(L^{1})$_2$]** and $PhSiH_3$, in CD_3CN.

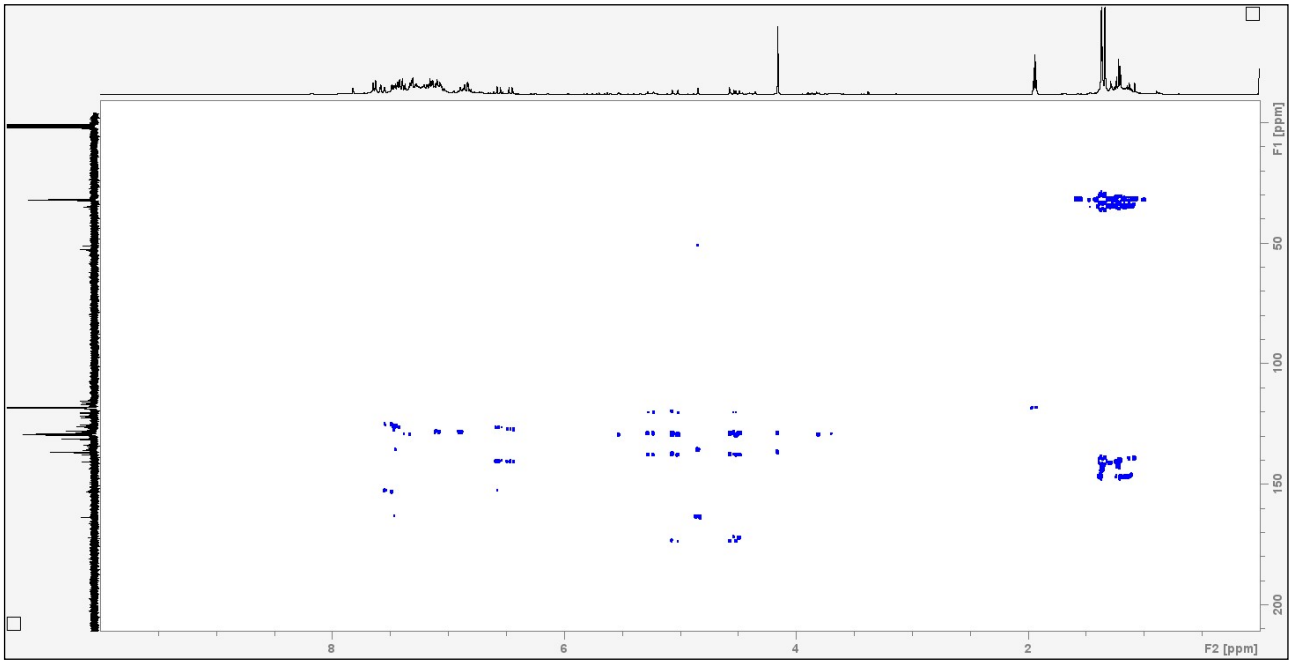

Figure S52. 2D NMR HMBC ^{13}C–^{1}H spectra of the reaction between **[Cu(L^{1})$_2$]** and $PhSiH_3$, in CD_3CN.

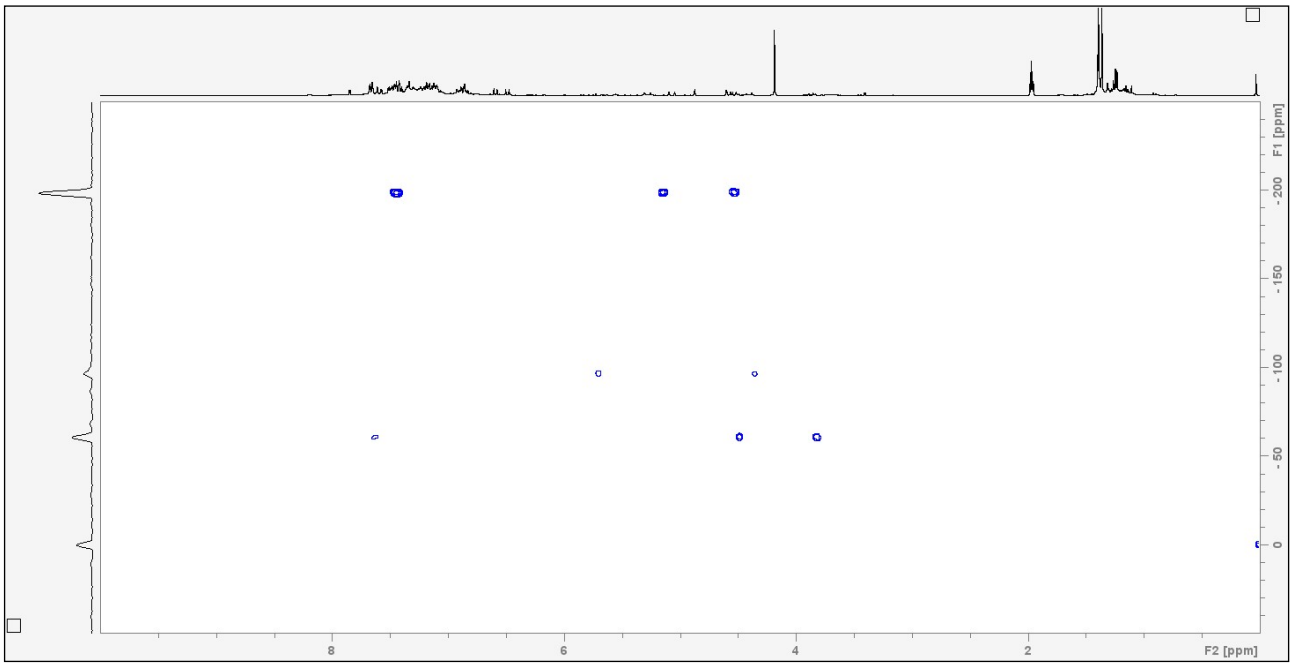

Figure S53. 2D NMR HMBC ^{29}Si–^{1}H (without J_1 suppression) spectra of the reaction between **[Cu(L^1)$_2$]** and $PhSiH_3$, in CD_3CN.

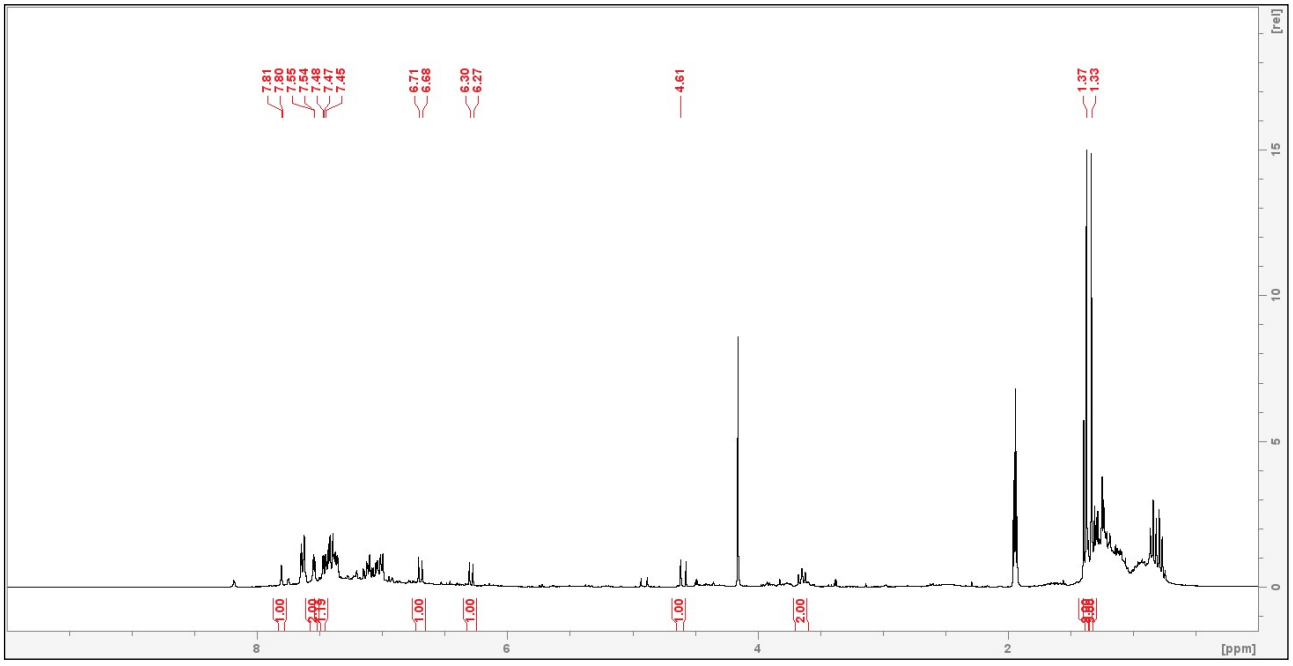

Figure S54. ^{1}H NMR spectra of the reaction between **[Cu(L^2)$_2$]** and $PhSiH_3$, in CD_3CN.

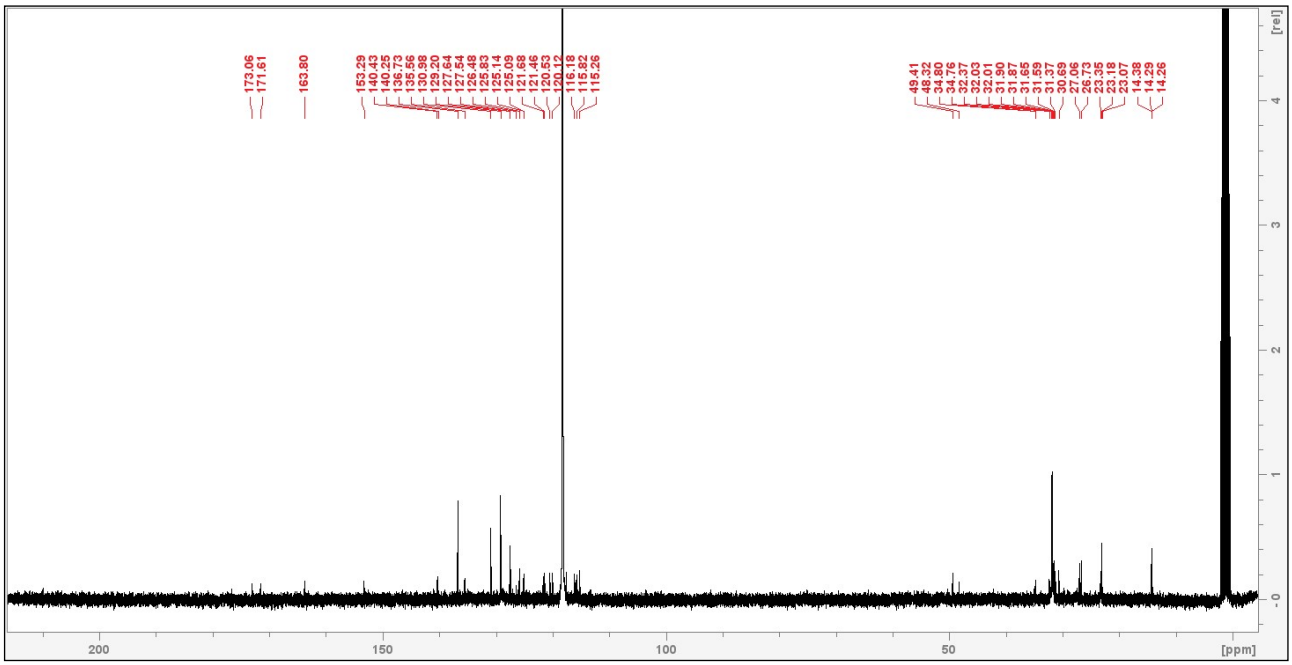

Figure S55. ^{13}C NMR spectra of the reaction between **[Cu(L^2)$_2$]** and $PhSiH_3$, in CD_3CN.

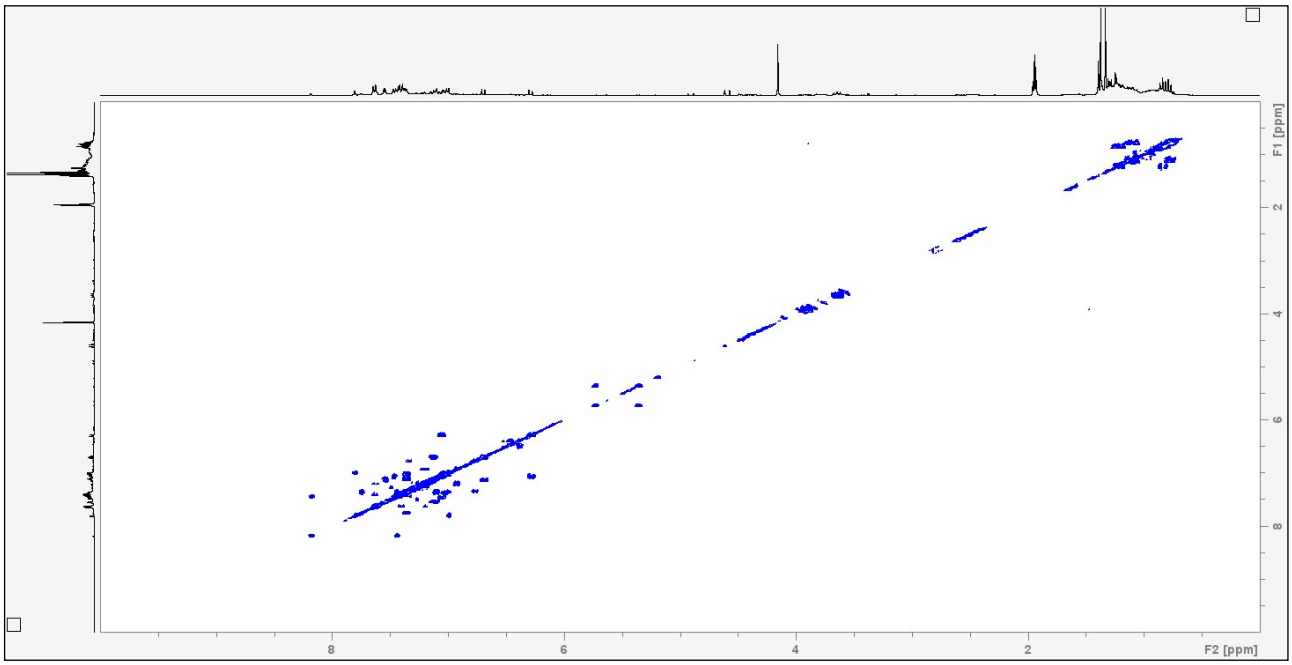

Figure S56. 2D NMR COSY ^1H–^1H spectra of the reaction between **[Cu(L^2)$_2$]** and $PhSiH_3$, in CD_3CN.

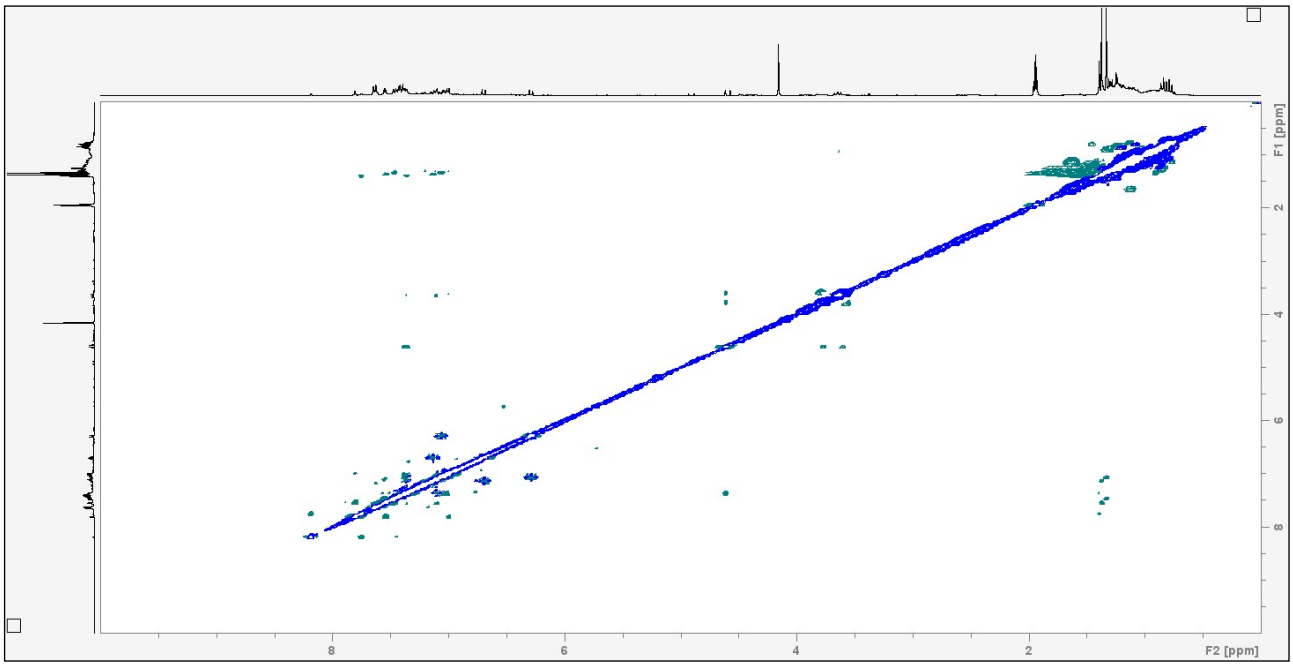

Figure S57. 2D NMR NOESY ^{1}H–^{1}H spectra of the reaction between **[Cu(L^{2})$_{2}$]** and $PhSiH_3$, in CD_3CN.

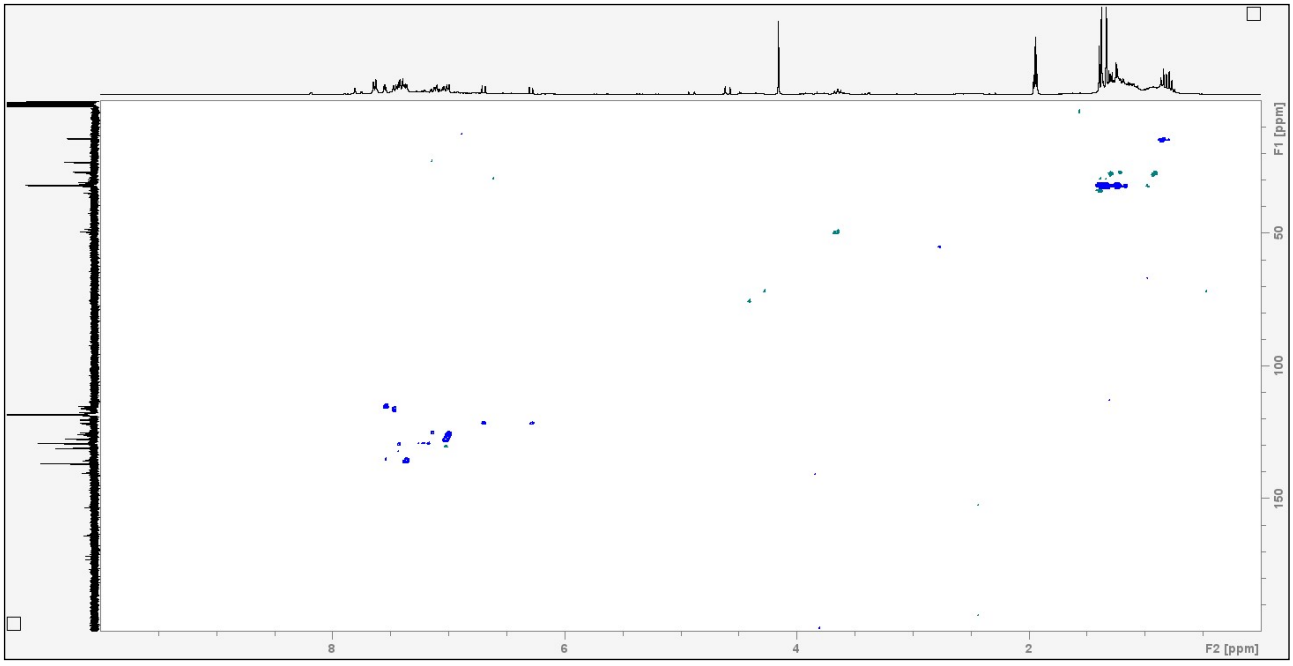

Figure S58. 2D NMR HSQC INEPT ^{13}C–^{1}H spectra of the reaction between **[Cu(L^{2})$_{2}$]** and $PhSiH_3$, in CD_3CN.

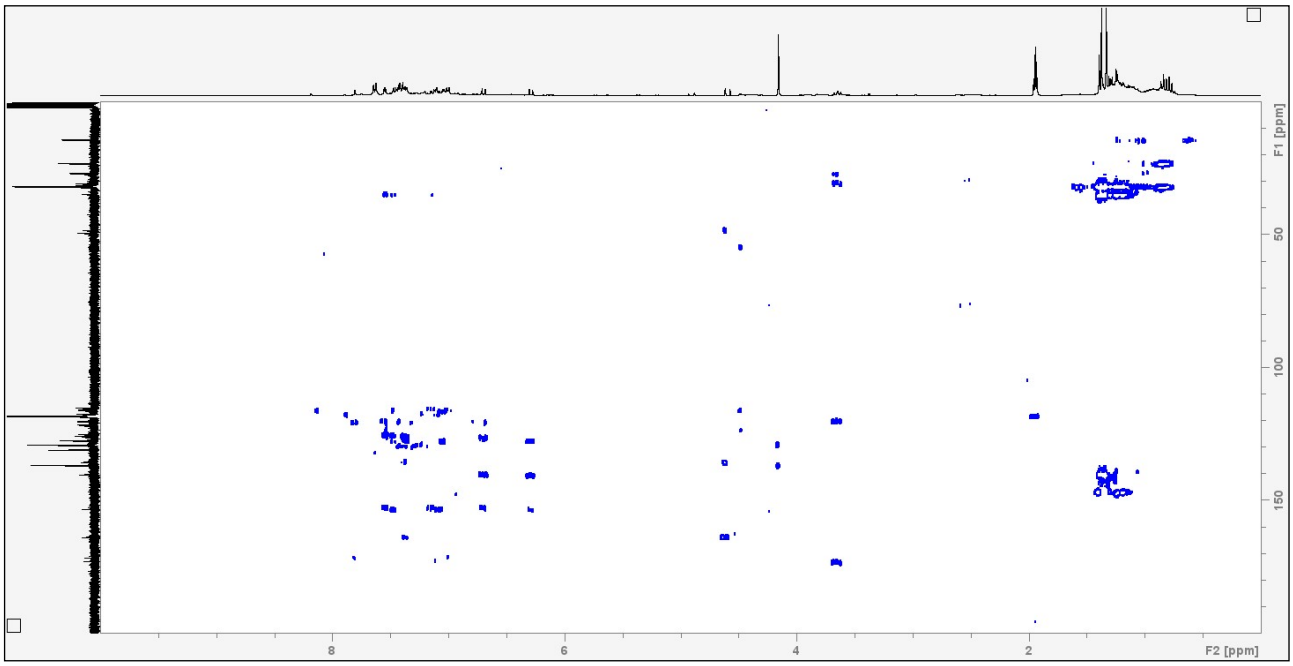

Figure S59. 2D NMR HMBC ^{13}C–^{1}H spectra of the reaction between **[Cu(L^{2})$_{2}$]** and $PhSiH_3$, in CD_3CN.

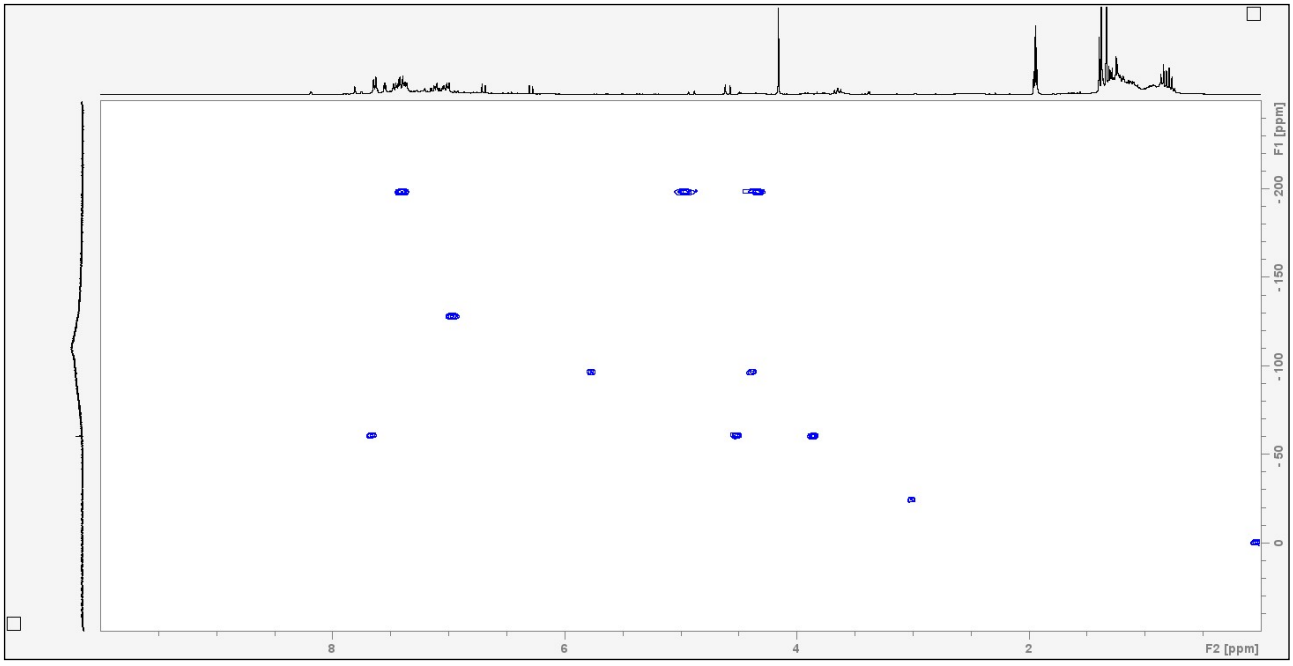

Figure S60. 2D NMR HMBC ^{29}Si–^{1}H (without J_1 suppression) spectra of the reaction between **[Cu(L^{2})$_{2}$]** and $PhSiH_3$, in CD_3CN.

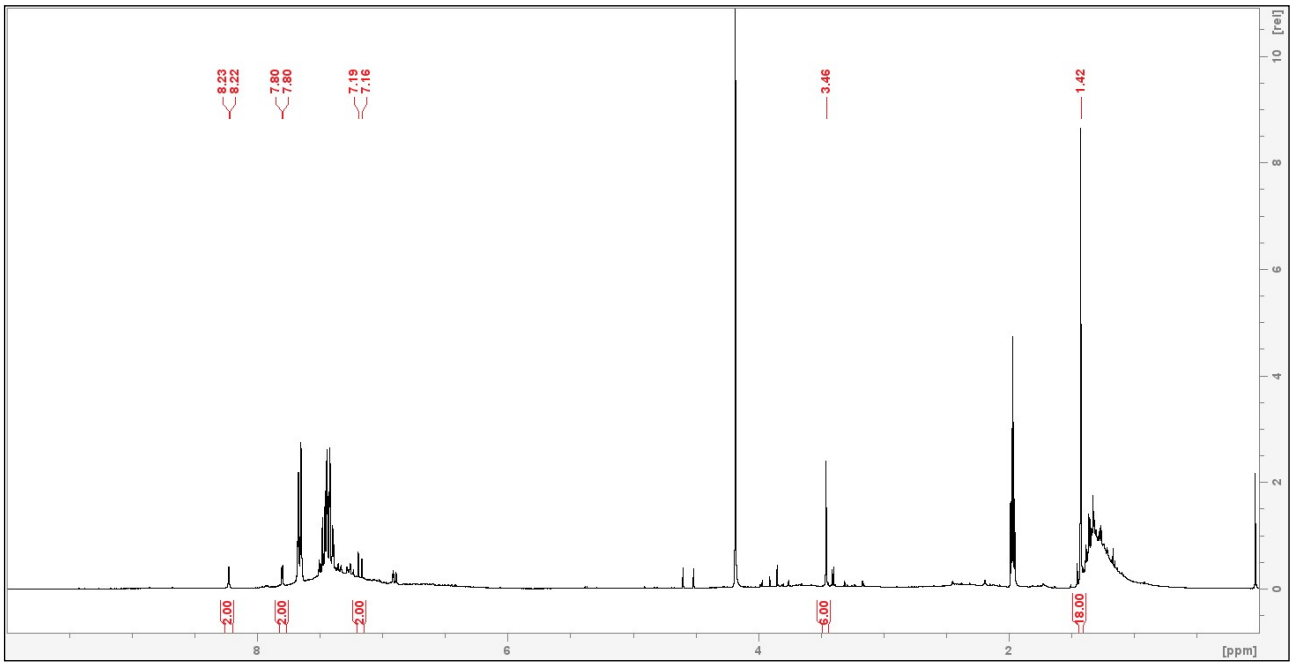

Figure S61. ^{1}H NMR spectra of the reaction between **[Cu(L^{3})$_{2}$]** and $PhSiH_3$, in CD_3CN.

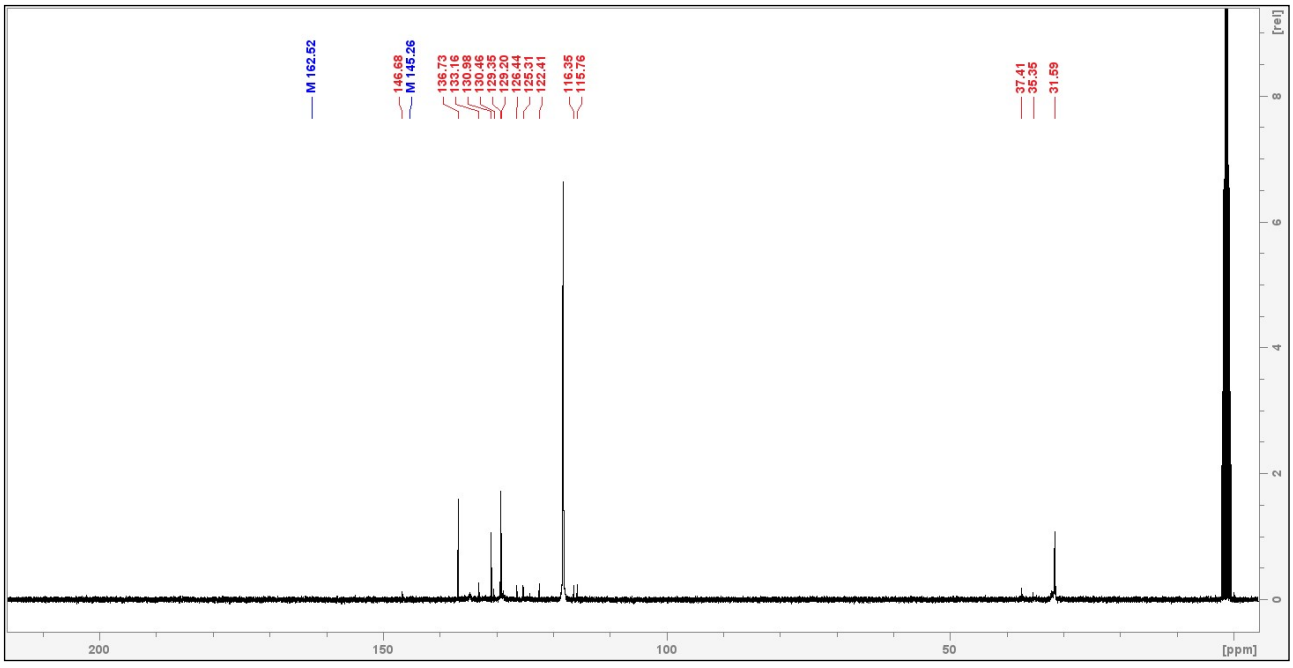

Figure S62. ^{13}C NMR spectra of the reaction between **[Cu(L^{3})$_{2}$]** and $PhSiH_3$, in CD_3CN.

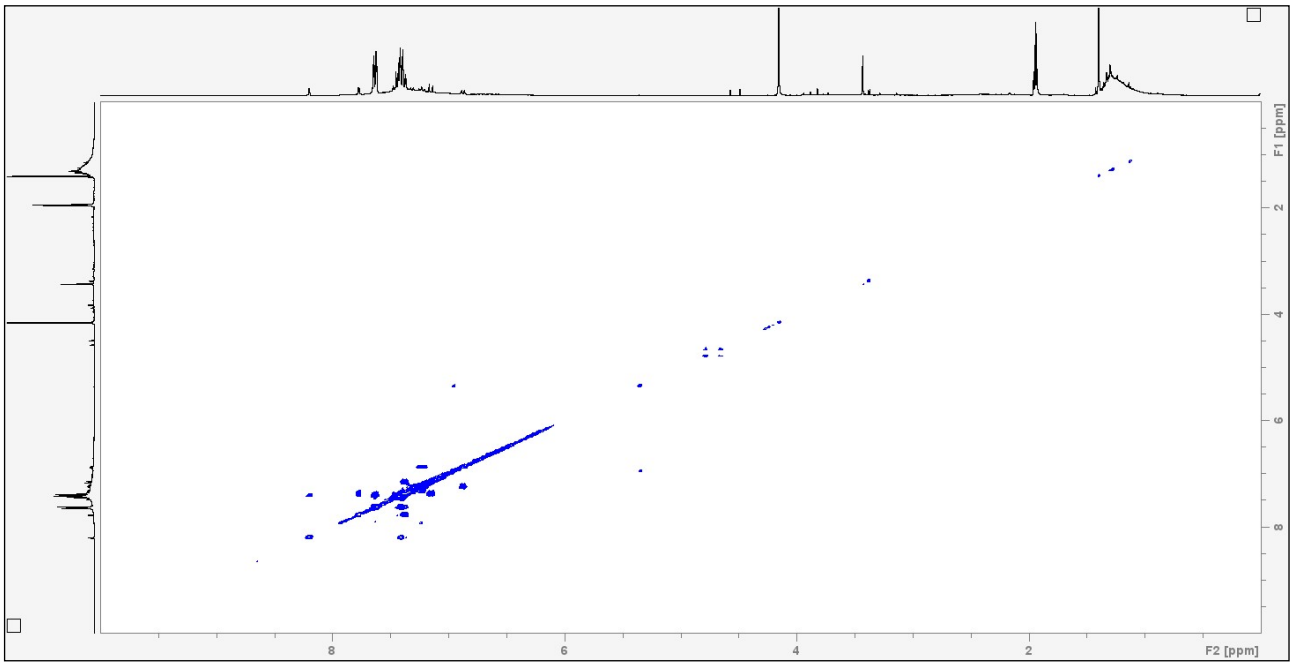

Figure S63. 2D NMR COSY ^{1}H–^{1}H spectra of the reaction between **[Cu(L^{3})$_2$]** and $PhSiH_3$, in CD_3CN.

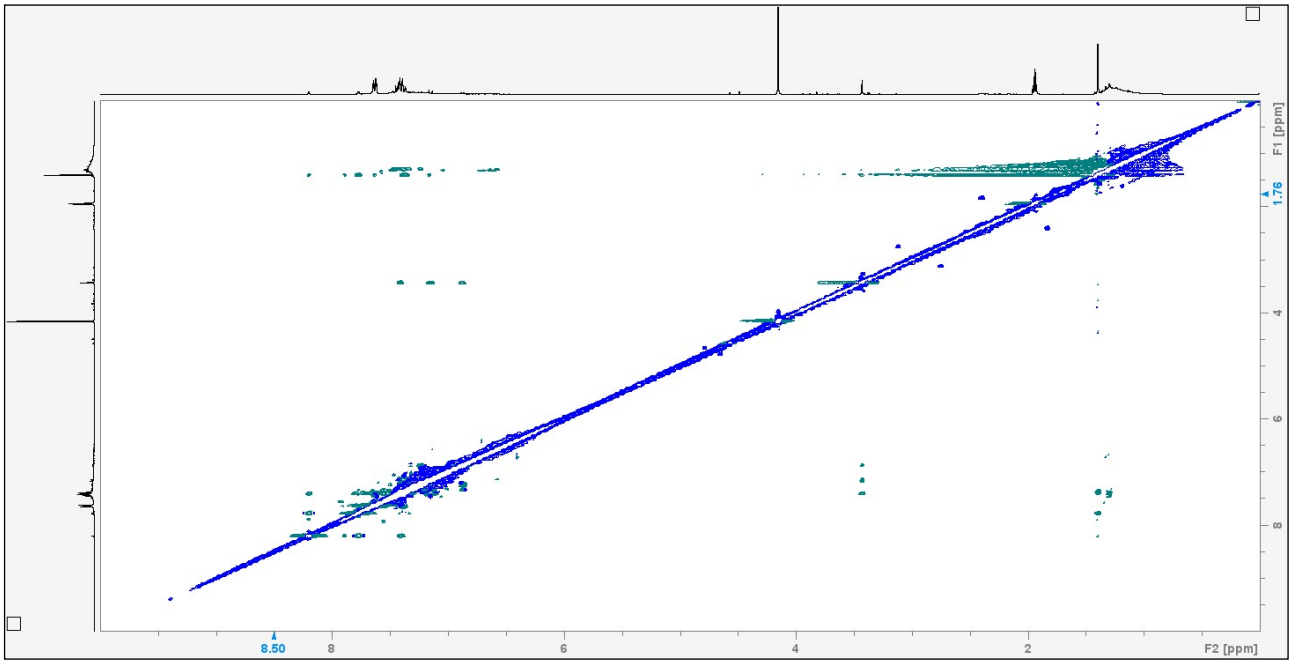

Figure S64. 2D NMR NOE ^{1}H–^{1}H spectra of the reaction between **[Cu(L^{3})$_2$]** and $PhSiH_3$, in CD_3CN.

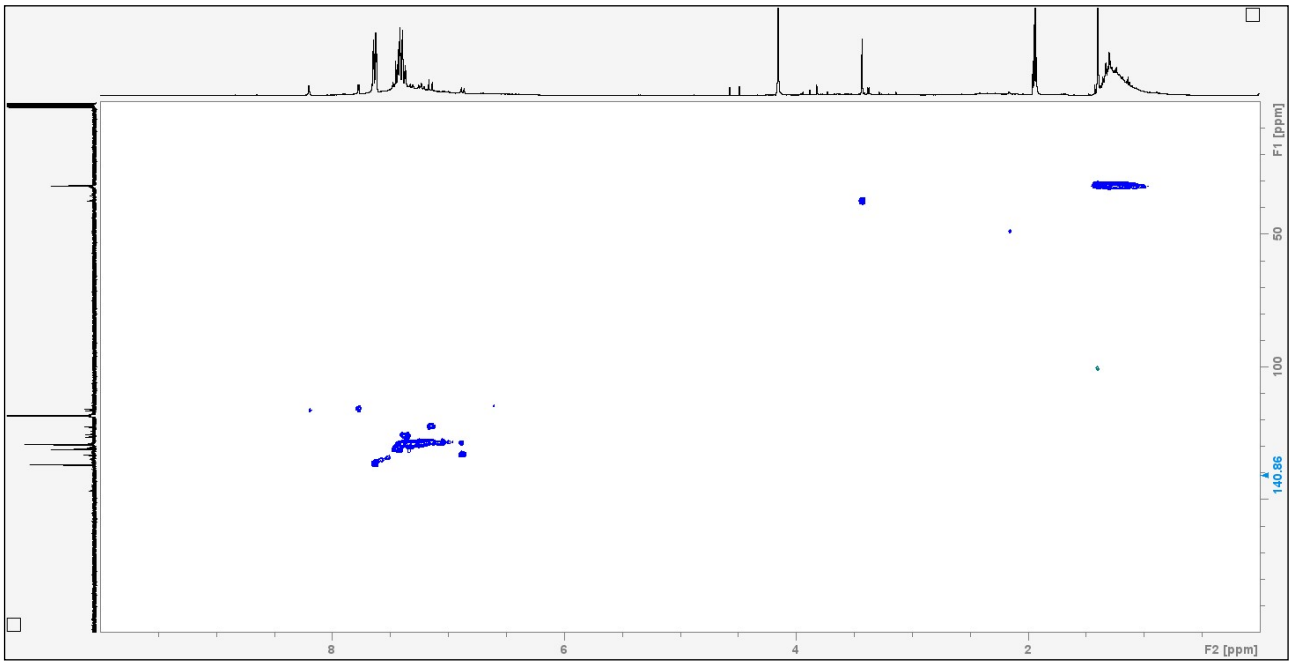

Figure S65. 2D NMR HSQC INEPT ^{13}C–^{1}H spectra of the reaction between **[Cu(L^{3})$_{2}$]** and $PhSiH_3$, in CD_3CN.

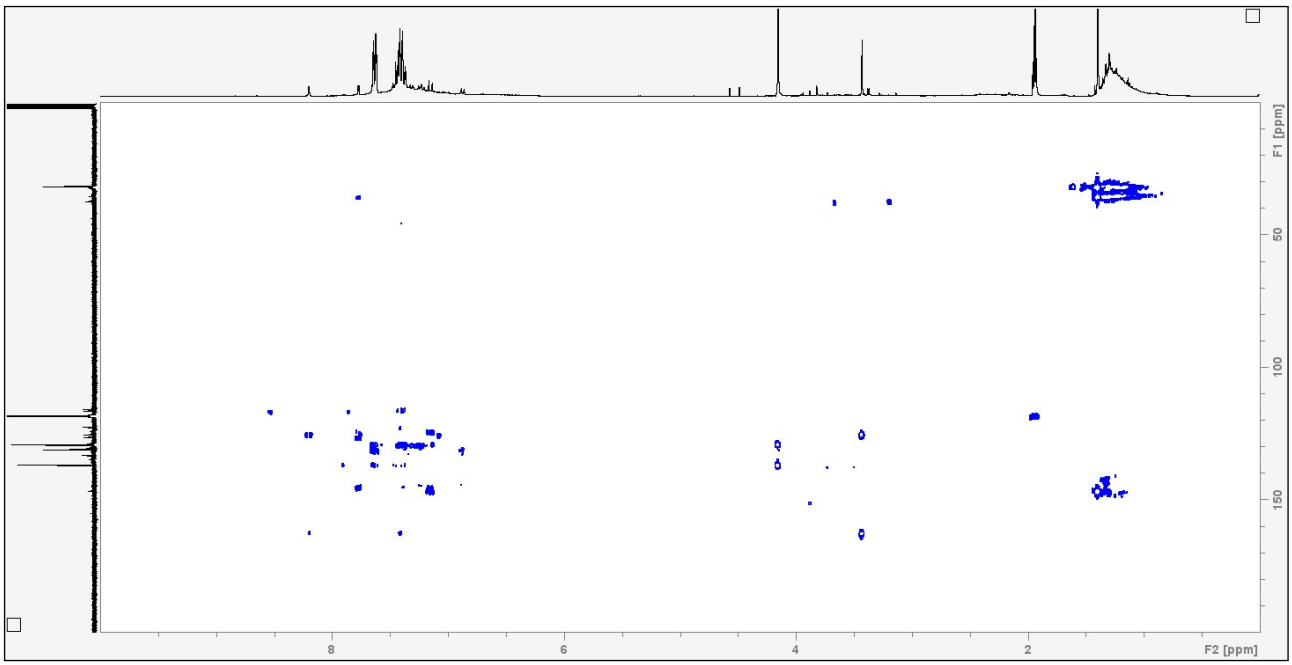

Figure S66. 2D NMR HMBC ^{13}C–^{1}H spectra of the reaction between **[Cu(L^{3})$_{2}$]** and $PhSiH_3$, in CD_3CN.

12. Computational details

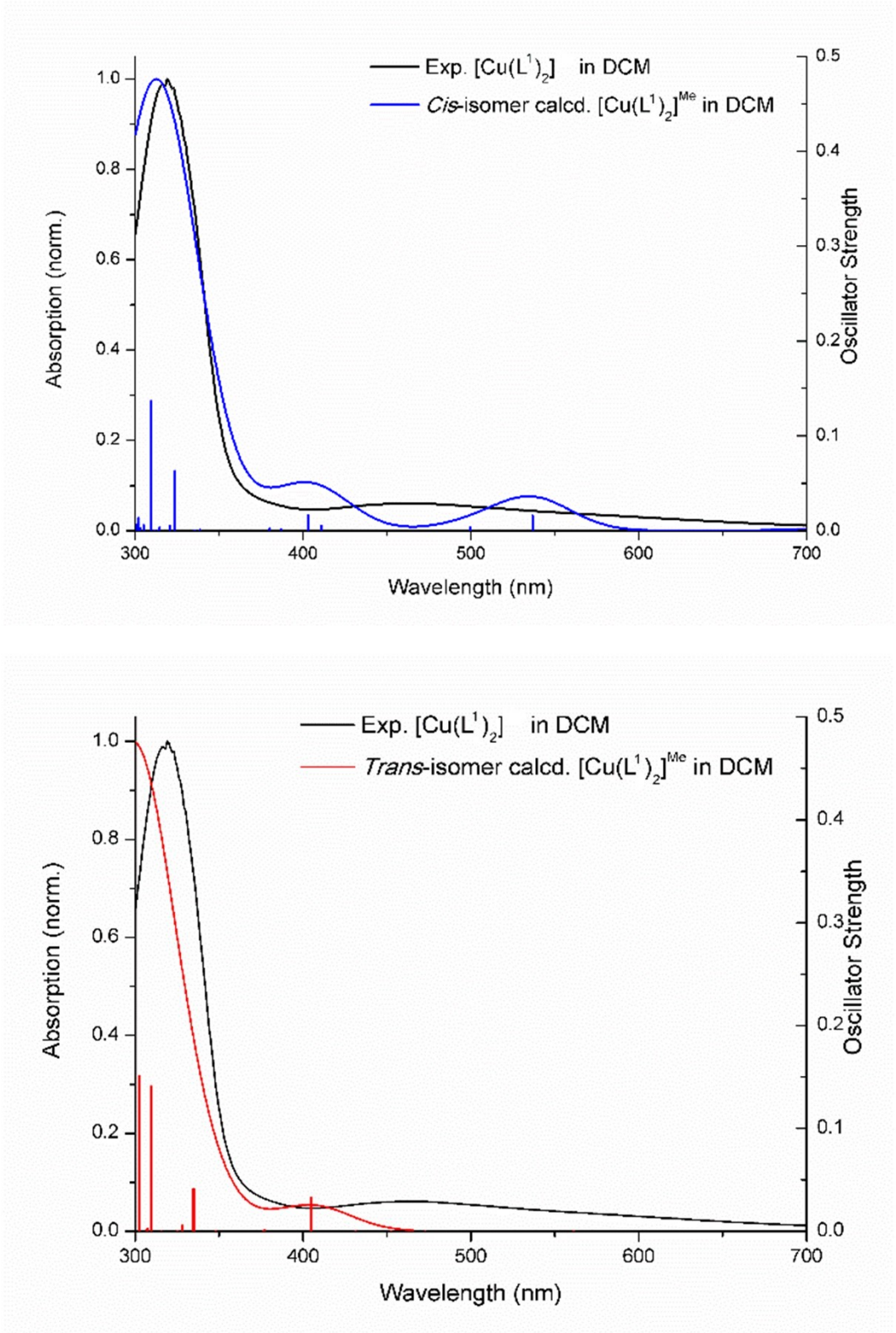

Figure S67. Predicted absorption spectra of ***cis*-[Cu(L^1)$_2$]^{Me}** (top) and ***trans*-[Cu(L^1)$_2$]^{Me}** (bottom) and comparison with the experimental spectrum of **[Cu(L^1)$_2$]**. Calculations at the TDDFT ZORA PBE0 ZORA-Def2-TZVPP D3BJ level of theory with inclusion of solvent effects for DCM with the CPCM method.

XYZ coordinates of **$[Cu(L^1)_2]^{Me}$ *trans*-isomer**

C	8.083474000	3.714977000	8.931058000	C	2.993034000	6.564519000	10.731060000
C	9.684907000	2.129227000	8.924663000	C	2.672549000	5.210355000	10.566927000
H	10.408884000	1.453227000	8.487980000	H	3.418628000	4.547987000	10.126826000
C	9.348327000	2.357852000	10.217819000	C	1.438335000	4.728139000	10.993878000
H	9.693338000	1.888383000	11.127923000	H	1.198946000	3.673067000	10.868496000
C	8.966768000	2.973487000	6.705386000	C	0.512331000	5.588373000	11.587919000
H	8.157943000	3.622220000	6.364591000	H	-0.451903000	5.207234000	11.921413000
H	8.790449000	1.953767000	6.342617000	C	0.828063000	6.934450000	11.759661000
C	10.295095000	3.488768000	6.216584000	H	0.112642000	7.609315000	12.227453000
C	10.614165000	4.843272000	6.380722000	C	2.064898000	7.418692000	11.331288000
H	9.867190000	5.504983000	6.820284000	H	2.313642000	8.471584000	11.471003000
C	11.848223000	5.326601000	5.954580000	C	5.565300000	6.243536000	5.571264000
H	12.086525000	6.381915000	6.080036000	C	6.890650000	5.750170000	5.670913000
C	12.775456000	4.467167000	5.361286000	C	7.525332000	5.442562000	4.441918000
H	13.739566000	4.849162000	5.028418000	H	8.562277000	5.112597000	4.485187000
C	12.461102000	3.120779000	5.189486000	C	6.873747000	5.557094000	3.225293000
H	13.177485000	2.446528000	4.722279000	H	7.409166000	5.298115000	2.310913000
C	11.224429000	2.635412000	5.617068000	C	5.538760000	5.982276000	3.145059000
H	10.976783000	1.582265000	5.477316000	C	4.909778000	6.324513000	4.339240000
C	7.721301000	3.808082000	11.375312000	H	3.869644000	6.648458000	4.312265000
C	6.395729000	4.300838000	11.275281000	Cu	6.643315000	5.025442000	8.472985000
C	5.760658000	4.608289000	12.504107000	N	8.368908000	3.333854000	10.205065000
H	4.723551000	4.937724000	12.460640000	N	8.897063000	2.957729000	8.160360000
C	6.412030000	4.494131000	13.720892000	N	4.918141000	6.717921000	6.741696000
H	5.876281000	4.752906000	14.635138000	N	4.390529000	7.094162000	8.786523000
C	7.747180000	4.069560000	13.801489000	O	5.771620000	4.477765000	10.145634000
C	8.376596000	3.727512000	12.607473000	O	7.514954000	5.572722000	6.800380000
H	9.416856000	3.403990000	12.634664000	C	4.821423000	6.055716000	1.826588000
C	5.203605000	6.336555000	8.015644000	H	5.364238000	6.684615000	1.108808000
C	3.939038000	7.694235000	6.729183000	H	4.715126000	5.062512000	1.369681000
H	3.593985000	8.163866000	5.819176000	H	3.815484000	6.474899000	1.940331000
C	3.602745000	7.922886000	8.022402000	C	8.464334000	3.996837000	15.120101000
H	2.879039000	8.599052000	8.459280000	H	7.919875000	3.370765000	15.839082000
C	4.321534000	7.078651000	10.241548000	H	9.469195000	3.574849000	15.007183000
H	4.498839000	8.098267000	10.604116000	H	8.573221000	4.990661000	15.575078000
H	5.130054000	6.429310000	10.581921000				

XYZ coordinates of **$[Cu(L^1)_2]^{Me}$ *cis*-isomer**

C	7.705078000	3.923621000	9.015696000
C	8.725097000	1.921875000	9.126304000
H	8.909718000	0.883344000	8.881730000
C	9.299632000	2.730268000	10.057506000
H	10.068923000	2.528445000	10.790016000
C	6.862431000	2.210868000	7.452407000
H	5.833511000	2.449532000	7.743406000
H	6.943437000	1.117603000	7.412796000
C	7.170939000	2.816840000	6.106933000
C	8.467593000	2.773352000	5.585311000
H	9.266119000	2.300355000	6.157878000
C	8.749533000	3.347129000	4.347634000
H	9.763337000	3.309654000	3.950868000
C	7.734123000	3.964553000	3.615749000
H	7.954722000	4.417336000	2.650368000
C	6.439045000	4.006139000	4.127777000
H	5.641534000	4.498634000	3.573968000
C	6.160773000	3.438888000	5.370248000
H	5.153913000	3.511922000	5.781658000
C	8.917906000	5.072599000	10.807328000
C	7.845436000	5.966635000	11.097727000
C	8.145856000	6.956688000	12.070649000
H	7.329925000	7.620852000	12.351086000
C	9.410815000	7.105311000	12.611158000
H	9.586776000	7.903930000	13.333773000
C	10.480573000	6.273596000	12.236647000
C	10.197496000	5.251430000	11.337103000
H	11.000851000	4.588088000	11.014305000
C	6.939305000	6.087449000	6.867629000
C	6.716779000	7.379082000	5.039583000
H	6.202984000	7.971289000	4.295903000
C	8.043699000	7.160740000	5.227446000
H	8.905032000	7.516964000	4.677193000
C	9.412397000	5.901958000	6.893992000
H	10.062646000	5.610921000	6.061322000
H	9.188293000	4.988403000	7.454610000
C	10.110855000	6.896349000	7.786842000
C	9.394725000	7.699341000	8.679123000
H	8.306632000	7.650155000	8.707463000
C	10.066895000	8.553142000	9.549713000
H	9.496431000	9.158024000	10.250922000
C	11.459866000	8.613366000	9.539991000
H	11.981737000	9.280752000	10.224273000
C	12.180741000	7.815164000	8.653863000
H	13.268931000	7.857899000	8.638401000
C	11.506576000	6.964026000	7.779300000
H	12.072663000	6.342783000	7.084015000
C	4.641755000	6.596570000	6.158852000
C	4.052393000	6.291600000	7.418200000
C	2.632583000	6.266829000	7.432022000
H	2.166776000	6.060389000	8.394039000
C	1.871509000	6.480006000	6.298227000
H	0.783948000	6.438545000	6.372879000
C	2.467167000	6.737235000	5.051315000
C	3.856361000	6.787982000	5.015336000
H	4.347523000	6.967574000	4.059087000
Cu	6.490695000	5.407999000	8.658253000
N	8.660901000	3.953830000	9.970530000
N	7.750946000	2.672668000	8.505171000
N	6.053540000	6.703675000	6.048307000
N	8.155121000	6.361142000	6.341386000
O	6.681351000	5.919058000	10.541271000
O	4.707744000	6.053775000	8.506591000
C	1.637044000	6.943830000	3.815930000
H	0.998248000	6.075216000	3.606828000
H	0.973933000	7.813591000	3.917302000
H	2.266358000	7.111201000	2.934408000
C	11.871866000	6.504331000	12.752454000
H	11.876200000	6.699268000	13.832265000
H	12.516564000	5.637622000	12.566763000
H	12.341093000	7.369506000	12.262118000

13. References

[1] A. Mondal, A. K. Suresh, G. Sivakumar, E. Balaraman, *Org. Lett*. **2022**, *24*, 8990–8995.

[2] X.-F. Li, X.-G. Zhang, F. Chen, X.-H. Zhang, *J. Org. Chem*. **2018**, *83*, 12815–12821.

[3] Z. Guo, T. Pang, L. Yan, X. Wei, J. Chao, C. Xi, *Green Chem.* **2021**, *23*, 7534–7538.

[4] G. Li, J. Chen, D.-Y. Zhu, Y. Chen, J.-B. Xia, *Adv. Synth. Catal.* **2018**, *360*, 2364–2369.

[5] A. E. Wahba, M. T. Hamann, *J. Org. Chem.* **2012**, *77*, 4578–4585.

[6] V. Kanaujiya, V. Tiwari, S. Baranwal, V. Srivastava, J. Kandasamy, *Synlett* **2023**, *34*, 970–974.

[7] T. A. Gokhale, S. C. Gulhane, B. M. Bhanage, *Eur. J. Org. Chem.* **2023**, *26*, e202200997.

[8] Z. Wang, S. Chen, C. Chen, Y. Yang, C. Wang, *Angew. Chem. Int. Ed.* **2023**, *62*, e202215963.